energies

MDPI

Article

Supercritical Water Gasification of Coconut Shell Impregnated with a Nickel Nanocatalyst: Box–Behnken Design and Process Evaluation

Marcela M. Marcelino [1], Gary A. Leeke [2], Guozhan Jiang [2], Jude A. Onwudili [3], Carine T. Alves [1,4,5], Delano M. de Santana [1,5], Felipe A. Torres [1,5,6], Ednildo A. Torres [1,5] and Silvio A. B. Vieira de Melo [1,5,*]

1 Programa de Engenharia Industrial, Escola Politécnica, Universidade Federal da Bahia, Rua Prof. Aristides Novis, 2, 6° Andar, Federação, Salvador 40210-630, Brazil; marcelamagalhaes16@yahoo.com.br (M.M.M.); carine.alves@ufrb.edu.br (C.T.A.); delano.mendes@ufba.br (D.M.d.S.); ftorres@ufrb.edu.br (F.A.T.); ednildo@ufba.br (E.A.T.)
2 School of Chemical Engineering, University of Birmingham, Birmingham B15 2TT, UK; g.a.leeke@bham.ac.uk (G.A.L.); g.jiang@bham.ac.uk (G.J.)
3 Energy & Bioproducts Research Institute, School of Infrastructure & Sustainable Engineering, Aston University, Birmingham B4 7ET, UK; j.onwudili@aston.ac.uk
4 Departamento de Engenharia de Energia, Centro de Ciência e Tecnologia em Energia e Sustentabilidade, Universidade Federal do Recôncavo da Bahia (UFRB), Feira de Santana 44085-132, Brazil
5 Centro Interdisciplinar em Energia e Ambiente (CIENAM), Campus Universitário Federação/Ondina, Universidade Federal da Bahia (UFBA), Salvador 40170-115, Brazil
6 Departamento de Sistemas Mecânicos, Centro de Ciências Exatas e Tecnológicas, Universidade Federal do Recôncavo da Bahia, Cruz das Almas 44380-000, Brazil
* Correspondence: sabvm@ufba.br

Abstract: The energy conversion of nickel-impregnated coconut shells using supercritical water has not yet been explored. The impregnation process was conducted at room temperature and a pH of 5.80 for 72 h. Characterization of the prepared sample confirmed the presence of nickel nanoparticles with an average size of 7.15 nm. The gasification of control and impregnated samples was performed at 400–500 °C, biomass loading from 20 to 30 wt% and residence time from 20 to 60 min. The response surface methodology (RSM) approach, with a Box–Behnken method, was used to design the experiments. The optimization model showed that the non-catalytic process at 500 °C, 60 min and 20 wt% of biomass loading could promote an H_2 yield of 8.8 mol% and gasification efficiency of 47.6%. The gasification of nickel-impregnated coconut shells showed significantly higher gasification efficiency (58.6%) and hydrogen yield (17.2 mol%) with greater carbon and hydrogen efficiencies (109.4 and 116.9%) when compared to the non-catalytic process. The presence of nickel particles in the biomass matrix as nanocatalysts promoted higher hydrogen production and supercritical water gasification efficiency.

Keywords: coconut shell; supercritical water gasification; hydrogen; efficiency; nickel

Citation: Marcelino, M.M.; Leeke, G.A.; Jiang, G.; Onwudili, J.A.; Alves, C.T.; Santana, D.M.d.; Torres, F.A.; Torres, E.A.; Vieira de Melo, S.A.B. Supercritical Water Gasification of Coconut Shell Impregnated with a Nickel Nanocatalyst: Box–Behnken Design and Process Evaluation. *Energies* **2023**, *16*, 3563. https://doi.org/10.3390/en16083563

Academic Editor: M. A. Fazal

Received: 31 March 2023
Revised: 14 April 2023
Accepted: 18 April 2023
Published: 20 April 2023

1. Introduction

For many years, studies have presented the harmful effect of fossil fuels on the planet with strong links to climate change and global warming. This is driving the increased use of renewable biomass resources, which are readily available, abundant and sustainable through the development of appropriate conversion technologies. Biomass has the potential to become a carbon-neutral and possibly carbon-negative resource to meet global energy demand, reduce our dependence on conventional (fossil) energy sources and improve access to clean and affordable energy [1].

Large quantities of solid biomass are generated from urban and agricultural activities. Brazil's tropical climate and high temperatures support a growing demand for coconut for use as food and beverages. According to the FAO, of the United Nations, in 2020,

2,458,839.00 million tons of coconut were produced in Brazil, thereby leading to a large amount of coconut residue waste generation, such as coconut shell, representing 60% of the coconut weight. This study used coconut shells as a biomass feedstock to produce energy. As a feedstock, this biomass source has several advantages, such as high availability, low price, low ash content, high lignin content, high calorific value and low density [2].

Energy can be obtained from coconut shells through thermochemical methods such as pyrolysis and gasification. Several authors have researched the pyrolysis of coconut shells, focusing on producing liquid and solid products [2–4]. Coconut shells have also been used as a feedstock for conventional gasification processes, aiming to produce synthesis gas [5–8]. However, the hydrothermal conversion processes of coconut shells through supercritical water gasification have been little explored by researchers [9–11].

The conversion of coconut shells to hydrogen-rich syngas through supercritical water gasification was performed by Nanda et al. [9]. The authors found that using coconut shell with 2 wt% of homogenous catalyst (K_2CO_3) at 600 °C and a 1:10 biomass-to-water ratio for 45 min resulted in a superior hydrogen yield. A similar process was performed by Wang et al. [11], focusing on obtaining biochar. During the tests, a homogeneous catalyst (K_2CO_3) was used. In their results, the authors found that biochar presented better characteristics when compared to that traditionally obtained by pyrolysis.

Supercritical water gasification (SCWG) is an innovative alternative to convert biomasses with high moisture content into H_2-rich syngas. In the supercritical condition (T > 374.29 °C and p > 22.089 MPa), water behaves as a homogeneous and organic non-polar phase. Thus, the water becomes completely miscible with gases and hydrocarbons. These properties favor homogeneous reactions with organic compounds during SCWG [12,13].

Homogeneous and heterogeneous catalysts have been used on enhanced supercritical water gasification with natural biomass feedstock. Nevertheless, most research efforts have focused on using a heterogeneous catalyst due to advantages such as high selectivity towards specific gas products (e.g., hydrogen or methane), recyclability and reusability, which make the SCWG process environmentally friendly. For high hydrogen yields, nickel is a commonly used heterogeneous catalyst due to its ability to catalyze C–C bond breaking and improve the influence on the water–gas shift reaction [14]. However, using nickel-based catalysts on various supports (e.g., silica, carbon and other metal oxides) presents operational challenges such as hydrothermal instability, loss of activity via poisoning, phase transformation and susceptibility to sintering and carbon deposition [14–16]. The wet impregnation of biomass with nickel nanocatalysts represents a viable alternative to surpass the issues originating from the classical supported process, improving the catalytic activity and hence the efficiency of SCWG and the quality of the gas product.

Recent studies have employed this approach to impregnate nickel catalysts into different biomasses for subcritical and supercritical water gasification [17–20]. In the non-catalytic process, Nanda et al. [20] related that the SCWG of wheat straw at 500 °C and a 1:10 biomass-to-water ratio produced gas yields and CGE (carbon gasification efficiency) higher than those found on SCWG of pinewood biomass. For the authors, it occurred due to pinewood biomass fibrous characteristics. Kumar and Reddy [18] investigated the SCWG of mosambi peels and sugarcane bagasse under non-catalytic conditions at 500 °C and a 1:8 biomass-to-water ratio. The authors concluded that the total gas, hydrogen yield and CGE value were lower for the mosambi peels biomass due to its high lignin content. Biomasses with larger cellulose and hemicellulose yields gasify easily. Lee et al. [14] reported that the high lignin content contributes slightly to the gas formation by interfering with the cellulose decomposition process via inhibition of the decarbonylation reactions and favoring the dehydration reactions.

All of the reported results by the authors indicated that the gasification of nickel-impregnated biomasses leads to higher total gas and hydrogen yields and greater carbon gasification efficiency compared to the non-catalytic process. This is due to the potential of nickel nanoparticles to catalyze reactions, such as reforming and the water gas shift

reaction and promote the degradation of straight chain and ring compounds, enhancing gas yield [17–20].

These studies have also shown how operational factors SCWG of the biomass through the classic one-factor-at-time (OFAT) experimental approach, in which one variable is changed. In contrast, the other factors are kept constant [21]. Conversely, the response surface methodology (RSM) effectively fits the experimental results and optimizes the process. Through this method, many factors are varied concomitantly and prudently [21,22]. The Box–Behnken experimental design has been used to approximate a response function to experimental data. Authors have presented evidence about the advantages of using this practical approach, such as the highest economical and efficiency [23]. The literature reports only a few studies about RSM applied to supercritical water gasification [16,21,22,24]. However, there is currently no research on parameter optimization in SCWG of coconut shells using the RSM method based on the Box–Behnken design.

Despite the positive influence on the characteristics of the gaseous products and process efficiency, studies focusing on the SCWG of impregnated biomasses with nickel nanocatalysts are uncommon in the literature [17–20]. Moreover, the effect of heterogeneous catalysts on the SCWG of coconut shells and the impregnation of this biomass with nanocatalysts are aspects that have never been reported. Thus, it is necessary to develop practical applications to improve scientific knowledge about the mechanisms involved and evaluate the performance of the catalytic supercritical water gasification process.

Therefore, this current study focuses on integrating nickel metal into the coconut shell to produce H_2-rich syngas and enhance gasification efficiency. The biomass was characterized and the effect of nickel nanocatalysts on the gasification process was investigated in detail. The assessment of the effects of SCWG process variables (temperature, biomass loading and reaction time) on the gas composition produced from coconut shells was performed. The RSM based on a Box–Behnken design was employed to model the independent variables and demonstrate the optimum condition for obtaining maximum hydrogen and gasification efficiency.

2. Materials and Methods

2.1. Material and Chemicals

Brown coconut shell biomass was obtained from Bahia Orchidarium, Camaçari, Bahia, Brazil. The biomass samples were crushed through a ball mill to a particle size < 1 mm. Then, the biomass was sieved to obtain a range of size from 45 to 90 µm and oven-dried at 105 °C to eliminate moisture and allow its physicochemical characterization. The chemicals used for impregnation were acquired from ThermoFisher, Altrincham, Cheshire, United Kingdom. Nickel (II) nitrate hexahydrate [$Ni(NO_3)_2 \cdot 6H_2O$, 99.99% purity] was used as a metal precursor, whilst nitric acid and ammonia solution were used to keep the proper solution pH for promoting the metal association into the biomass.

2.2. Identification of the pH_{ZPC} Value

The pH solution is an important parameter that needs to be analyzed in order to improve the nickel loading and dispersion in the biomass [16]. At the zero-point charge (pH_{ZPC}), determined by the pH drift method, the maximum loading of nickel is reached. In order to determine the pH, a glass electrode was used after being calibrated.

The influence of the solution pH on nickel loading should be studied to optimize both metal loading and dispersion in the biomass matrix [16]. Maximum loading of the metal is attained at the pH where the zero-point charge (pH_{ZPC}) is present in the solution, and it was determined using the pH drift method. In the catalyst impregnation procedure, 10 mL of a known 0.1 M concentration of nickel salt solution was prepared by pH regulation in the 2–10 range using either nitric acid or ammonia solution to investigate the metal loading process. Next, a mass ratio of 1:10 catalyst/biomass was used to adjust the pH of the nickel salt solution and mixed with a magnetic stirrer at 300 rpm for 24 h. Then, the final pH of all biomass samples was plotted against the initial pH to calculate pH_{ZPC}. In order to identify

the pH_{ZPC} value, the pH value where the curve crosses the initial pH = final pH line was considered [18,25].

The impregnated biomass was filtered by a vacuum and washed with deionized water. After that, samples were dried at 40 °C for 3 days. For moisture removal, samples were oven-dried at 105 °C.

2.3. Biomass Sample Preparation

At the p_{HZPC} value, about 50 g of coconut shell biomass and 500 mL of nickel salt solution (1.0 M concentration) were mixed. The solution was kept on a magnetic stirrer at 300 rpm for 72 h. After impregnation, the impregnated sample was filtered by a vacuum system and washed with deionized water. The sample was dried at 40 °C for 3 days and further at 105 °C for 8 h for final moisture removal [20]. A control sample was also produced by mixing 50 g of coconut shell biomass with 500 mL of deionized water under analogous stirring rates, stirring times, sample filtration and drying conditions.

These prepared samples were analyzed to determine their physicochemical properties before performing supercritical water gasification experiments.

2.4. Investigation of Biomass Characteristics

The impregnated and control biomass samples were characterized by adopting various analytical methods, such as proximate analysis, ultimate analysis, TGA/DTG (thermogravimetric/derivate thermogravimetry), SEM-EDX (scanning electron microscopy-energy dispersive X-ray spectroscopy), X-ray diffraction (XRD) and FTIR (Fourier transform infrared spectroscopy).

The proximate analysis of the samples was determined according to ASTM E1756-08 (moisture), ASTM E1755-01 (ash) and ASTM D 5832-98 (volatile matter), including moisture).

Fixed carbon was calculated by Equation (1), given by

$$\text{Fixed Carbon} = 100 - [\text{volatile } (\%) + \text{ash } (\%)] \quad (1)$$

The elemental analysis of the samples, such as amounts of C, H, N and S, was determined by a Flash 2000 Elemental Analyzer CHNS analyzer. Oxygen (weight percent) was calculated by difference as

$$O = 100 - (C + H + N + S + Ni) \quad (2)$$

A thermogravimetric analyzer carried out thermal degradation (TGA/DTG) of impregnated and control biomass (Model-EXSTAR 6000, TG/DTA6300, Birmingham, UK). In each analysis, approximately 10 mg of the biomass was placed in an appropriate crucible, then heated from 50 to 900 °C at a heating rate of 10 °C/min in a nitrogen (N_2) atmosphere (flow rate of 100 mL/min).

A scanning electron microscope (JEOL JSM-6060LV, Low Vacuum SEM, Birmingham, UK), coupled with an energy dispersive X-ray analyzer EDX spectroscope (OXFORD INSTRUMENTS INCA X-ACT, Model–51-ADD0058, High Wycombe, UK), was employed for determining the morphology and element composition of control and impregnated samples. Samples were prepared using a Quorum Emscope SC500 Sputter Coater.

For XRD analysis of the samples, a Bruker D8 Advance diffractometer was used, with Cu Kα1,2 radiation. The samples were top-loaded into PMMA specimen holders and the diffractograms were collected in the Bragg–Brentano geometry with a step scan of 0.02° (1 s per step). Organic functional groups associated with the control and impregnated samples were determined by a FTIR spectrometer (Model-JASCO FT/IR-6300, Cremella, Italy) in the wavelength range 600–4000 cm^{-1}, coupled with Jasco Spectra Manager™ II software.

2.5. Supercritical Water Gasification Experiments

2.5.1. Reactor Assembly

The gasification experiments were performed in a tube batch reactor. The tube reactor was constructed using Swagelok fittings and 1/2″ 316 stainless steel tubing with a wall thickness of 0.065″. The total volume of the reactor (including fittings) was 10 mL. A K-type thermocouple was installed at the bottom of the reactor, and a sampling valve and a pressure gauge were installed at the top. All accessories used in the assembly were made up of stainless steel (SS 316) and purchased from Swagelok (Swagelok Bristol, England, UK).

The reactor was initially loaded with predefined amounts of water and biomass to ensure that after the furnace (ELITE THERMAL SYSTEMS LIMITED, Market Harborough, UK) heated the tubular reactor to the desired temperature, the system could reach the desired pressure. Then, the reactor and lines were purged with N_2 to remove any air. The schematic of the reactor and the heating procedure is presented in Figure 1.

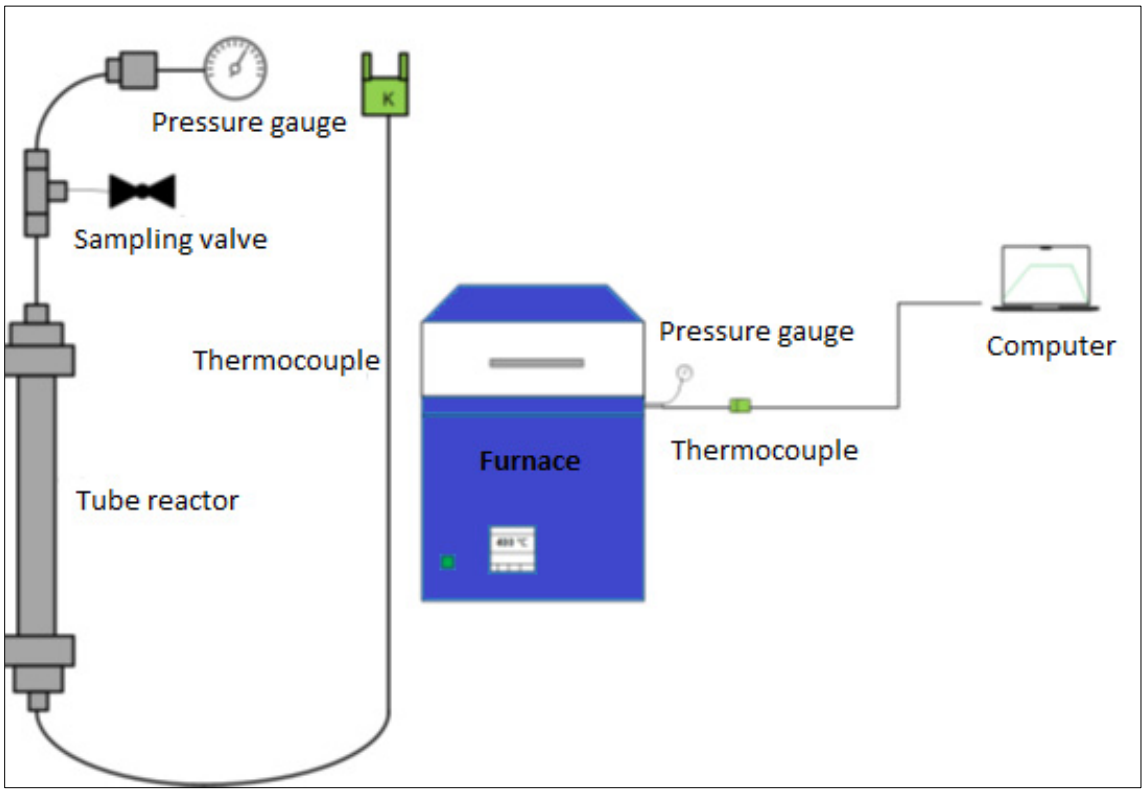

Figure 1. Schematic of the tube reactor and SCWG process.

The furnace was pre-heated to the reaction temperature to attain a satisfactory reactor heating rate and reduce the effect of thermal transients. The temperature was determined by a K-type thermocouple type K connected to a computer with Picolog 6.2.5 software installed. Once the supercritical pressure and temperature conditions were achieved, the sample was maintained for an established residence time, favoring the sample degradation into fuel gases. After the reaction, the reactor was quenched at ambient temperature (20 °C). The pressure was reduced to ambient, and the reactor's outlet valve was opened to separate the products in a gas–liquid separator composed of calcium chloride dihydrate and glass wool. This way, the moisture in the product gas was captured and trapped, and the moisture-free gas was collected in 30279-U inert foil gas sampling bags (obtained from Supelco, Poole, UK, 3) for analysis using gas chromatography.

After the gas sampling, the reactor was opened to collect the liquid residuals, which were transferred into a glass container and weighed. The moisture content in the gas product was determined by the difference in weight of the gas–liquid separator, which

was measured before and after each experimental run. This value was added to the quantification of liquid products. The solid material was eliminated by washing the reactor many times with acetone. A vacuum system was used to filter the acetone-solid mixture. Then, the solid content was established as the difference between the weights of filter papers. The diagram illustrating the product collection is presented in Figure 2.

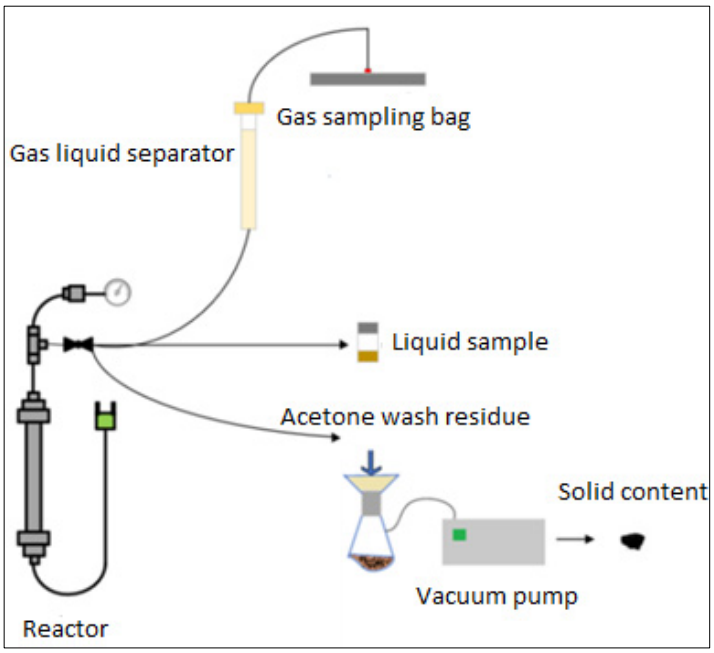

Figure 2. Representation of the solid and liquid samples collection.

2.5.2. Experimental Design

The RSM method, using a 3-level and 3-factor Box–Behnken, designed the experimental runs for studying the conjunct effects of different process variables on the gas yield produced by the SCWG of coconut shells. The influence temperature (400–500 °C), residence time (20–60 min) and biomass loading (20–30%) on the produced gas constituents was determined at a pressure range of 23 to 28 MPa. The concentrations of the gaseous product (H_2, CH_4, CO and CO_2) and gasification efficiency (GE) were investigated as response variables. In order to design the experimental runs, model and optimize the results, Design Expert Software (version 7.0, Stat-Ease Inc., Minneapolis, MN, USA) was used.

Equation (3) was used to determine the number of experiments requested for the Box–Behnken design [23].

$$N = 2k(k - 1) + c_p \quad (3)$$

where k is the number of factors and c_p is the number of central points.

A total of 15 experiments were conducted for each set of samples (impregnated and control samples). To investigate the experimental error, 3 replicates of the central point were performed. Table 1 shows the process variables and the coded and actual values for designing the experiments.

Table 1. Independent variables and their ranges used in Box–Behnken design.

Coded Values	Temperature (°C)	Residence Time (min)	Biomass Loading (wt%)
−1	400	20	20
0	450	40	25
1	500	60	30

2.6. Performance and Gas Analysis

The experimental results were investigated according to Equations (4)–(7). The molar fractions of each component in the gas product [26] were obtained using Equation (4):

$$\text{Molar fraction, } x_i\ (\%) = \frac{\text{the number of moles of each component}}{\text{the total number of moles}} \times 100 \quad (4)$$

The efficacy of the SCWG process was investigated through the evaluation of gasification efficiency (GE), carbon gasification efficiency (CGE) and hydrogen gasification efficiency (HGE), using Equations (5)–(7) below [27,28].

$$\text{GE}\ (\%) = \frac{\text{mass of gaseous products (g)}}{\text{mass of biomass (g)}} \times 100 \quad (5)$$

$$\text{CGE}\ (\%) = \frac{\text{the total mass of element carbon in the gaseous product (g)}}{\text{the total mass of element carbon in biomass}} \times 100 \quad (6)$$

$$\text{HGE}\ (\%) = \frac{\text{the total mass of element hydrogen in the gaseous product (g)}}{\text{the total mass of element hydrogen in biomass}} \times 100 \quad (7)$$

The collected moisture-free gas mixture was analyzed using a gas chromatograph system (GC-2014 Shimadzu, Buckinghamshire, UK) with a packed column (ShimCarbon ST) and a detector based on thermal conductivity (TCD). Hydrogen, carbon monoxide, carbon dioxide and methane were separated on a 200 m length by 0.35 mm inner diameter column. For each analysis, 1 µL of the gas sample was injected into the GC using a gas-tight syringe. The injector was held at 150 °C and the detectors at 100 °C. The column oven was programmed with an initial temperature of 45 °C. The total analysis time was 12 min.

3. Results and Discussion

3.1. Optimization of pH

In aqueous solutions, the components of the lignocellulosic biomass get protonated or deprotonated, which allows the presence of charges, increasing the number of accessible sites for metal impregnation. The pH of the solution has the capacity to improve metal loading. Thus, it is necessary to consider the proper pH_{ZPC} for improving the meal loading for the gasification process [18].

The influence of the solution pH on metal impregnation can be explained by the fact that there is competition among H^+ with heavy metal ions through a combination of mechanisms: ion exchange and the formation of surface metal complexes. This competition is enhanced at low pH; thus, the metal uptake is lower. The increase in pH value makes this effect less intense, and heavy metal ions are eliminated easily [29].

As shown in Figure 3, it was found a pH_{ZPC} value of 5.80 for coconut shell biomass. This graph agrees with the literature in which the pH_{ZPC} values for lignocellulosic biomasses are in the acidic range [16,30].

According to Kleinübing et al. [29], surface sites are protonated, and the surface becomes positively charged when pH values are reduced. When the pH is lower than pH_{ZPC}, low nickel uptake occurs due to the higher accumulation of H^+ ions in the solution, which competes with the metal species $[Ni(H_2O)_6^{2+}]$. When the pH increases towards the pH_{ZPC} value, nickel impregnation increases due to negative charge density on the coconut shell and favorable electrostatic attraction between positive species and biomass particles [16].

Based on this information, the impregnation process was carried out at a 5.80 pH value to reach a large metal loading and dispersion into the coconut shell matrix.

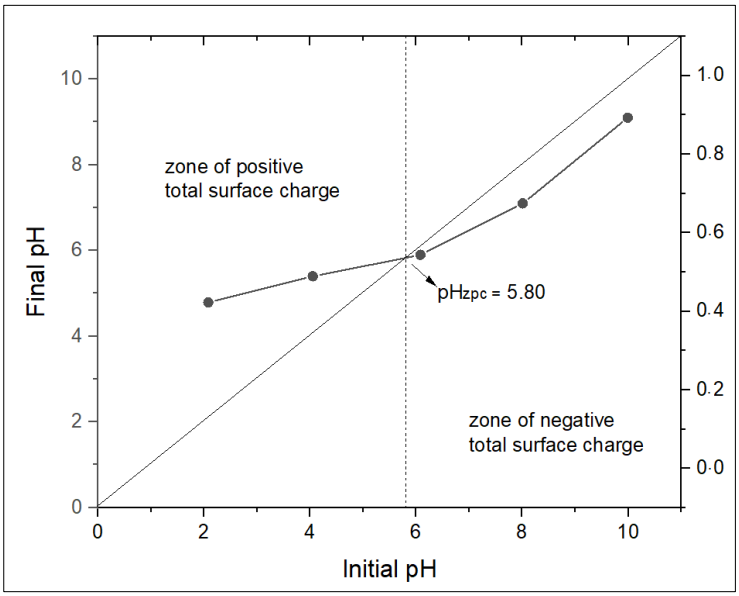

Figure 3. Zero-point charge of coconut shell biomass by pH drift method.

3.2. Characterization of Biomass

3.2.1. Proximate and Ultimate Analysis

As presented in previous studies in the literature [18,19], significant differences were not reported between the results of the proximate analysis of the impregnated and control samples. Hence, only the results obtained for control samples are discussed in this section.

Proximate analysis of the coconut shell was performed to determine the moisture, ash, volatile matter and fixed carbon contents. The results are shown in Table 2.

Table 2. Proximate analysis of coconut shell.

Proximate Analysis (wt%)	
Moisture	3.2
Volatile matter	77.5
Ash	2.9
Fixed carbon	19.6

According to data presented in Table 2, coconut shell was found to have a moisture content of 3.2%, a volatile matter of 77.5%, 2.9% of ash and about 19.6% of fixed carbon. Similar results were detected in recent reports about coconut shell characterization [1,11,31].

The findings of this study infer that coconut shell biomass is a good combustible source to produce energy products more efficiently due to low ash and moisture content. The high amounts of volatile matter and fixed carbon will positively affect gasification since coconut shell is easy to ignite at low temperatures and more char will be burned as combustible, increasing the energy yield and process efficiency [32,33].

The ultimate analysis of the samples is in Table 3. The results are presented on a dry and ash-free basis wt%.

Table 3. Ultimate analysis of control and nickel-impregnated biomass.

Parameter	Control (wt%)	Impregnated (wt%)
C	49.0	45.8
H	6.2	5.5
N	0.3	0.8
O	44.5	46.4
S	nd	nd

The elements determined from the analysis of the control sample were as follows: carbon, 49.0%; hydrogen, 6.2%; nitrogen, 0.3%; and oxygen, 44.5%. For impregnated samples, this was 45.8% of carbon, 5.5% of hydrogen, 0.8% of nitrogen and 46.4% of oxygen. The difference in both samples is attributed to the oxygen difference. No sulfur was detected in the coconut shell samples.

According to Table 3, it is possible to infer that carbon is the dominant component in the control sample (49.0%). However, in the impregnated sample, oxygen is the main component (46.4%). A comparable result was obtained in the study by Nanda et al. [20]. For the authors, the decrease in the carbon content of an impregnated sample results from incorporating water-soluble extractives into the metal salt aqueous solution, integrating hydrated or hydroxylated species of metal salts added to the increased amount of oxygen in the impregnated sample.

After the impregnation process, biomass hydrogen content decreased (from 6.2 to 5.5%). This results from deprotonating oxygenated surface groups and replacing at least one hydrogen atom with nickel metal ions from the hydroxyl group of macromolecules. The rise in nitrogen content is due to the incorporation of nickel nitrate $NiNO_3^+$ and ammonium NH_4^+ cations [16].

All results from the ultimate analysis corroborate that nickel was incorporated into the coconut shell biomass. The metal dispersion will promote the formation of small nickel particles during supercritical water gasification, promoting reactions that enhance gas yield and process efficiencies.

3.2.2. TGA/DTG Thermogravimetric/Derivate/Differential Thermogravimetric Analysis

The thermal decomposition characteristic of control and impregnated samples was investigated by performing TGA, DTG and DTA, which present an association between weight loss and temperature. The thermograms are shown in Figure 4.

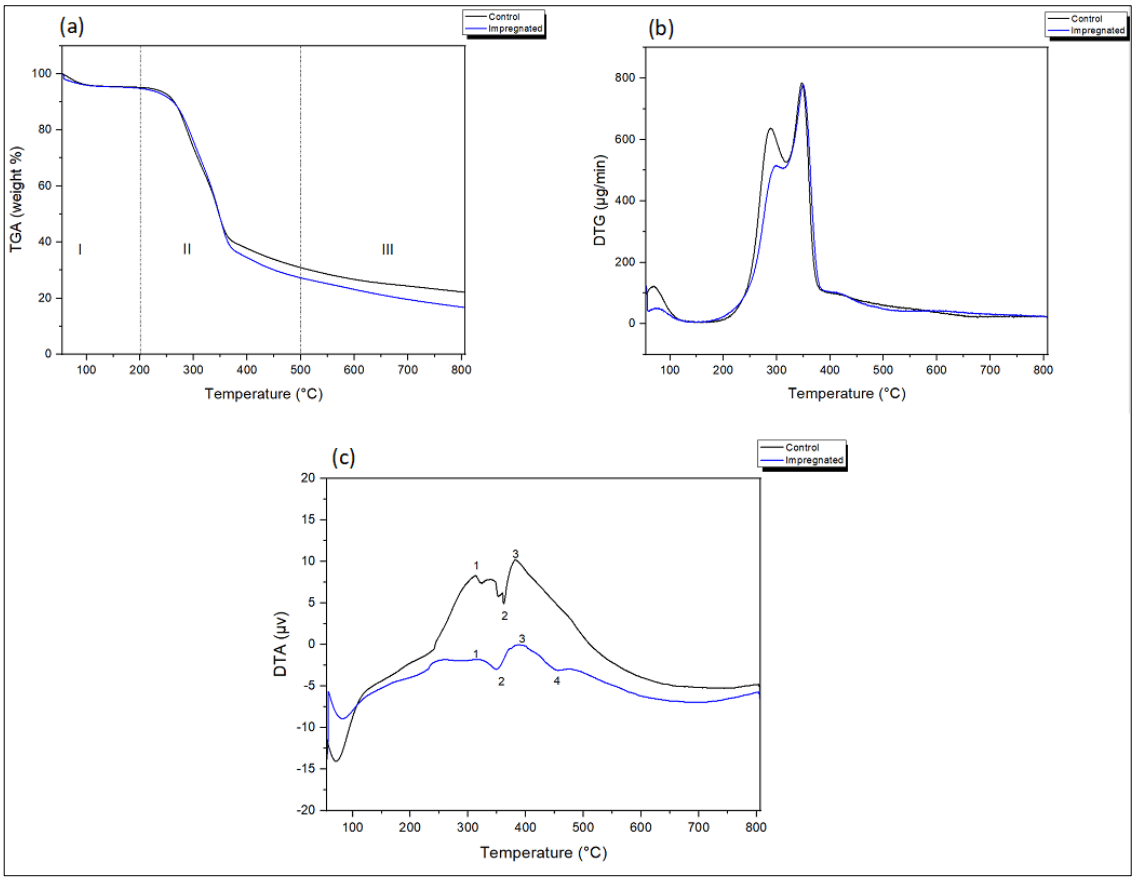

Figure 4. TGA (**a**), DTG (**b**) and DTA (**c**) of control and impregnated samples.

As can be seen from Figure 4a, impregnated and control samples were degraded into three particular phases. The initial phase (I) (up to 150 °C) is attributed to the moisture loss (at about 100 °C) and decomposition of less volatile compounds. The second stage (II) corresponds to devolatilization (between 150 and 500 °C), and in the last stage (III) (>500 °C), the shape is due to char/tar degradation. The distinction between the TGA curves of the samples is a consequence of the reductions of hemicellulose, cellulose and lignin amounts in the impregnated sample. The impregnation of the biomass with nickel at acidic pH (5.80) for 72 h possibly originated the degradation of the biomass structure [34].

Figure 4a also shows that the maximum weight loss was noticed in the 200–500 °C samples. In this phase, a slow degradation was observed, indicating char formation. The impregnated sample degradation resulted in higher weight loss (84.0%). In contrast, a lower weight loss of 78.6% was observed for the control sample. According to Nanda et al. [20], this may be from the catalytic action of nickel on the thermal degradation of biomass increasing the overall reaction rate at higher temperatures. The final residual material was approximately 15 and 22% of the initial mass for impregnated and control samples. Impregnated samples leave a lower quantity of char due to increased devolatilization in the presence of the nickel nanoparticles. Moreover, it was noticed that the TGA curves of control and impregnated samples intersect each other at 350 °C. From this temperature, nickel nanoparticles were produced, improving biomass degradation and decreasing char generation [19].

From the DTG curve, it is possible to indicate the thermal decomposition of biomass components better. Figure 4b shows that the first peak occurred between 50 and 120 °C, for both samples, indicating the weight loss due to moisture. The most noticeable peaks were found between the temperature ranges of 200–317 °C and 317–380 °C for control and impregnated samples, representing the degradation of hemicellulose and cellulose, respectively. Lignin was supposed to degrade at 200–500 °C but tended to continue through a much larger temperature range. The impregnated sample detected a lower mass loss from 50 to 380 °C due to the loss of water and decomposition of $Ni(OH)_2$ to NiO and H_2O [35]. Figure 4b also demonstrated the higher effect of nickel on char and tar degradation from 600 °C.

The differential thermograms shown in Figure 4c exhibit three peaks. The peaks at approximately 300 and 400 °C (peaks 1 and 3) are exothermic and represent the hemicellulose and lignin degradation for both samples. A sharp endothermic peak at about 350 °C (peak 2) is attributed to cellulose degradation. The DTA curve of the impregnated sample presents a different endothermic peak at 455 °C (peak 4). According to previous experiments developed by Richardson et al. [16], this peak's presence is due to Ni nanoparticle formation. This endothermic peak can be associated with reducing the Ni^{n+} species to metallic Ni by amorphous cellulose and hemicellulose carbon atoms, generally occurring between 400 and 500 °C [20,36,37]. For this temperature range, thermodynamic calculations infer that NiO reduction occurs to Ni [16]. Therefore, this temperature range is recommended for catalytic supercritical water gasification experiments.

3.2.3. SEM-EDX-Scanning Electron Microscopy-Energy Dispersive X-ray Spectroscopy Analysis

Figure 5 represents the SEM-EDX spectra for the impregnated sample.

The EDX spectra of the impregnated sample displayed the occurrence of carbon (58.9 wt%), oxygen (38.2 wt%) and alkali metal aggregates such as Al (0.5 wt%) and Si (0.9 wt%).

Richardson et al. [16] reported a significative loss of alkali cations in the impregnated sample. According to the authors, it results from the cation-exchange mechanism in the nickel incorporation process. The contents of carbon and oxygen detected by EDX are higher than those obtained by the ultimate analysis. This could be due to the non-detection of nitrogen, sulfur and hydrogen composition by EDX analysis [1].

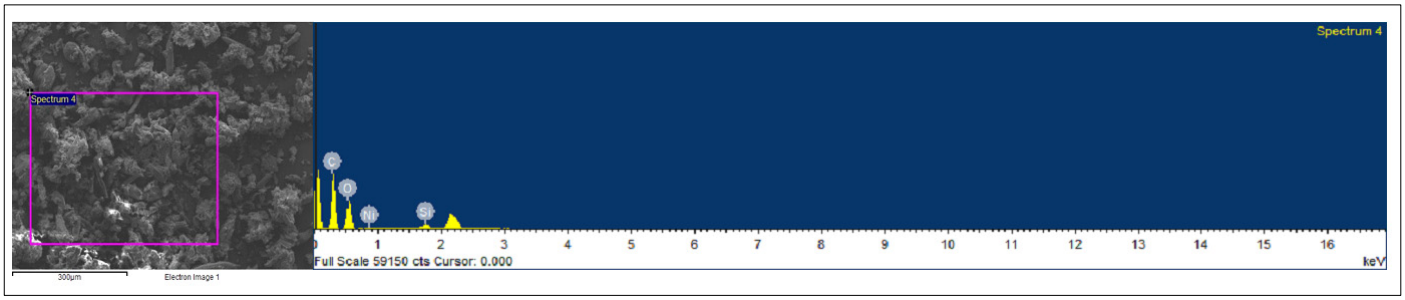

Figure 5. SEM-EDX spectra of impregnated sample.

The SEM image exhibited in Figure 5 shows clusters of nickel particles deposited on the surface. The coarse and conglomerate appearance of impregnated sample means that NiO nanoparticles were enclosed in biomass, demonstrating the amorphous character of the samples [26]. A characteristic nickel peak was observed at 0.88 keV in the impregnated sample. A similar result was obtained for impregnating pinewood and sugarcane bagasse [18,20].

In this study, a concentration of nickel of 1.6 wt% was obtained by coconut shell impregnation. After a similar impregnation processes, Richardson et al. [16] and Nanda et al. [20] reported 2.0 wt% and 1.2 wt% of nickel in impregnated woody and wheat straw samples, respectively. Higher nickel content (22.5 wt%) was reported by Kumar and Reddy [19] in impregnated banana pseudo-stem. The fibrous nature of some kinds of biomass, such as coconut shells, can result in a low loading of metal, which can affect the catalytic performance during the thermochemical process.

3.2.4. XRD-X-ray Diffraction Analysis

Figure 6 shows the XRD pattern of control and impregnated samples. The patterns reveal that the significant diffraction peaks are located at 16.26°, 21.72°, 26.32°and 34.47°. These peaks correspond to amorphous cellulose (I) and crystalline cellulose (II) [18,38,39].

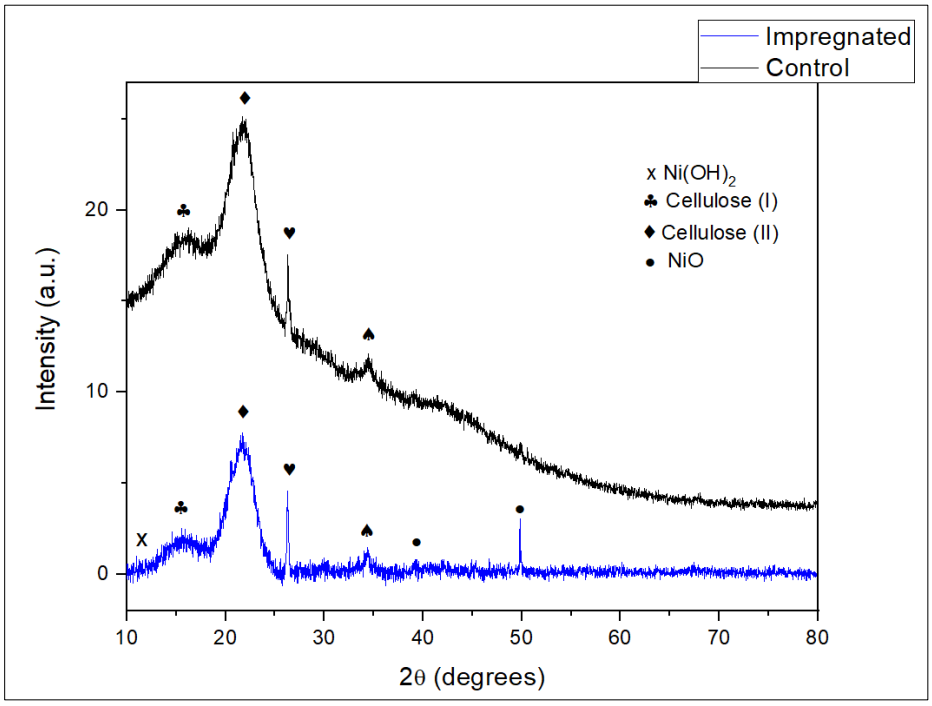

Figure 6. XRD pattern of control and impregnated coconut shell samples.

Compared to the impregnated sample, the amorphous region presented a reduction from 16.26°, 26.32° and 34.47° to 15.56°, 26.31 and 34.39°, respectively, while the crystalline region shifted from 21.72° to 21.80°, indicating increased incorporation of nickel. The impregnated sample shows diffraction peaks at 10.95°, 39.24° and 49.86°, which confirms of the presence of nickel nanoparticles in hydrated and oxide forms [16,18].

Nanomaterials can be characterized through many different techniques. From the XRD data exhibited in the plot, it is possible to know the size of the particle. The crystallite size diameter (L) of the nickel nanoparticles can be calculated by Scherrer's equation presented in Equation (8) [40]:

$$L = \left(\frac{k \cdot \lambda}{\beta(2\theta) \cdot \cos\theta} \right) \quad (8)$$

where k is the Scherrer constant (its value is most commonly taken as 0.9), λ is the wavelength of the X-ray used (0.15405 nm for Cu Kα radiation), β is the full width at half maximum of the peak and θ is the Bragg angle, both in radians [41,42].

The average crystallite size of the metal nanoparticles is around 7.15 nm in the impregnated samples, which reveals the presence of dispersed Ni particles at the nanoscale level (<100 nm) [43]. The literature has reported the formation of nickel nanoparticles spread into biomass matrices, ranging from 10 to 80 nm sizes [16,18,19]. The smaller particle size is a beneficial characteristic, which means a higher surface contact area, higher degree of dispersion and more extensive catalytic activity. Authors have reported that nanocatalysts with a larger number of active sites show better performance on a mass basis than micro-particle catalysts in the gasification process [44].

3.2.5. FTIR–Fourier Transform Infrared Spectroscopy

FTIR spectroscopy of control and impregnated samples was executed to identify the vibration frequency profiles in their functional groups within the range 500–4000 cm^{-1}, as presented in Figure 7.

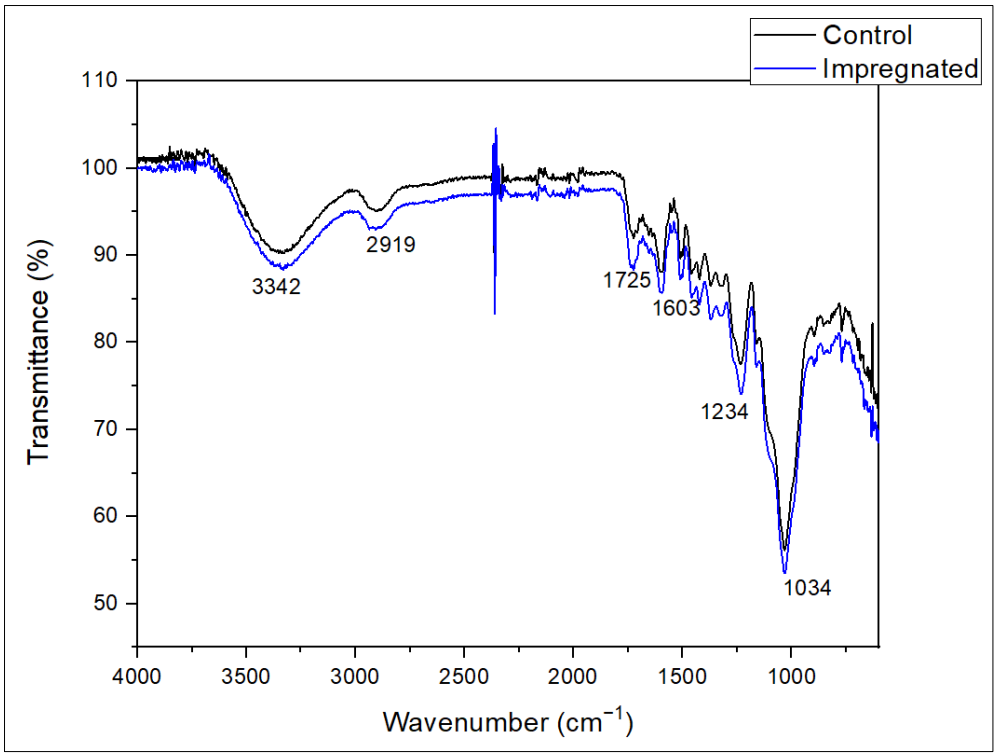

Figure 7. FTIR spectra of control and impregnated coconut shell samples.

The functional groups related to the peaks at different wavelengths were highlighted and elucidated conforming to literature data for coconut shell analysis [1,45–47].

For both control and impregnated samples, the band shifting around the broad peaks at 3342 cm^{-1} indicates the presence of hydroxyl groups (–OH), predominantly from hemicellulose and cellulose. The peaks at 2919 cm^{-1} are due to the CH stretching that causes CH, CH_2, and CH_3 group vibrations. The 1725 cm^{-1} peaks can result from an unconjugated carbonyl, probably due to uronic anhydrides. The peaks at 1603 cm^{-1} and 1234 cm^{-1} are due to C=C bond stretching in the benzene ring and C–O C–O stretching in C–OH phenolic groups, respectively.

Moreover, the modification at the peak of 3342 cm^{-1} and 2919 cm^{-1} exposed some vibrations of N–H and O–H, respectively. The peak at 1034 cm^{-1} represented the presence of silica, which is attributed to S–O stretching and bending. These findings agree with the results from the literature reports for agricultural biomass and nanocomposite materials [45,47].

3.3. RSM Experimental Design

For the RSM considering the Box–Behnken design, 15 experimental runs were executed for control samples. It admitted three factors at three levels, introducing the triplicate runs for the center points. The observed values and responses are presented in Table 4.

Table 4. Box–Behnken design and gas characteristics from supercritical water gasification of control coconut shell samples.

				Response Variables (%)				
Run	**A-Temperature (°C)**	**B-Residence Time (min)**	**C-Biomass Loading (wt%)**	**H_2**	**CO**	**CO_2**	**CH_4**	**GE**
1	450	20	20	7.1	3.9	58.6	30.4	30.3
2	500	60	25	7.3	0.9	48.7	43.2	40.1
3	450	60	20	6.5	1.3	64.2	28.1	40.4
4	500	40	20	8.3	0.5	48.3	43.0	52.0
5	450	40	25	4.2	4.1	67.0	24.8	24.0
6	450	40	25	1.7	3.9	62.8	31.7	21.3
7	400	20	25	4.5	9.0	75.8	10.7	18.8
8	500	20	25	9.5	3.2	40.7	46.8	33.9
9	450	40	25	5.8	4.6	64.5	25.1	32.0
10	450	20	30	1.8	5.4	73.7	19.2	27.0
11	450	60	30	3.8	1.1	69.1	26.0	37.8
12	500	40	30	5.8	0.3	38.5	55.5	48.8
13	400	40	30	0.2	4.8	78.8	16.2	25.5
14	400	40	20	5.5	5.5	74.1	14.9	26.5
15	400	60	25	2.3	5.8	74.9	13.8	25.9

According to the data in Table 4, during the SCWG process of the unimpregnated (control) sample, CO_2 was formed as the main gas with the largest value of 78.8 mol% at 400 °C, after 4 min of reaction and biomass loading of 30 wt% (run 13). The minimum value of 38.5 mol% of CO_2 was obtained at 500 °C with 30 wt% biomass loading and 40 min of reaction time (run 12). Temperature is a significant parameter affecting the product yield during biomass's thermochemical processing, including SCWG, notably when the reaction occurs without the catalyst [48]. Several authors have explained that high values of CO_2 yield at low temperatures are a consequence of the decarboxylation reaction that usually occurs at low temperatures [49,50].

As shown in Table 4, the maximum concentration obtained for CH_4 (55.5 mol%) was obtained from run 12, at 500 °C, 40 min and 30 wt%. At 400 °C and 25 wt%, the lowest concentration of CH_4 was obtained (10.7 mol%) in 20 min (run 7). Similar behavior was reported by Demirel, Erkey and Ayas [51,52]. They observed an increase in CH_4 content with temperature (0.3 mol/kg of CH_4 was obtained at 400 °C, whereas it was found to be

5.7 mol/kg at 600 °C). The amount of CH_4 increases with temperature by reason of the enhancement of methanation of CO and CO_2 reactions under this condition [52].

Table 4 shows that the greatest H_2 production of 9.5 mol% was detected at 500 °C with 25 wt% biomass loading during 20 min for run 8. The slightest amount of 0.2 mol% of H_2 was obtained at 400 °C with 30 wt% of biomass loading in 40 min (run 13). The highest amount of CO production (9.0 mol%) was obtained from run 7, where 25 wt% of biomass loading was gasified at 400 °C for 20 min. Despite this, the CO mole fraction was reduced to the minimum content of 0.3 mol% for 30 wt% biomass loading gasified at 500 °C for 40 min (run 12). The increase in CO yield at low temperatures and the favored formation of H_2 at a high temperature can be attributed to water gas-shift and steam reforming reactions that are dominant at high temperatures [53].

Gasification efficiency (GE) was also calculated as a response variable to investigate the performance of the SCWG process. From the data presented in Table 4, it is possible to infer that the highest GE value (52%) was attained at 500 °C with 20 wt% of biomass loading during 40 min of reaction (run 4). However, GE decreased to the lowest value of 18.8% during the gasification at 400 °C, residence time of 20 min and 25 wt% of biomass loading (run 7). The equivalent trend was observed by Chen et al. [22] in their SCWG experiments. According to these authors, the change after the increasing temperature is due to the shift from ionic to the free radical mechanism for biomass degradation, which enhances the reactions at higher temperatures, producing more gas. The next section of this study presents more details regarding the effect of process variables on gas composition and process efficiencies.

The effects of process variables on each constituent of produced gas (mol%) and gasification efficiency are expressed through ANOVA analysis and exhibited in Table 5.

The comparison between the variation resulting from the data treatment and the variation originating from the random errors related to the analysis of the produced responses is performed through ANOVA [23].

The large F values associated with low probability values demonstrate the high significance of the fitted model [54]. As shown in Table 5, the p values less than 0.0001 for CO_2 and CH_4, and 0.0011, 0.0001 and 0.0042 for H_2, CO and GE, respectively, confirm that the model is significant. The significance of the parameter in the process is related to the p value. Lower p values indicate a high significance of the parameter [54]. Thus, the variable temperature (A) was highlighted as the most significant in determining the composition of all gasification products and process efficiency. For CO and H_2, the residence time (B) and biomass loading (C) are also significant factors. Non-significant lack of fit is also an important statistical result, expressing that the mathematical model suits experimental data suitably [50].

In the normal probability graph presented in Figure 8, a straight line was observed, which indicates that residuals are normally distributed for the ANOVA results. Thus, we can consider that the ANOVA results are valid [54].

From the linear regression modeling, it was possible to establish quantifiable relations between the response variables and the process variables. The most significant model equations between the five variables and the responses are shown in Table 6. A, B and C are coded values of variables, including temperature, biomass loading and residence time, respectively. The equations, analysis of variance and experimental versus predicted analysis were obtained by using Design-Expert 7 (Stat-Ease, Inc., Minneapolis, MN, USA).

Table 5. ANOVA results for the model using the Box–Behnken design.

Source	H_2			CO			CO_2			CH4			GE		
	SS	**F**	***p***	**SS**	**F**	***p***	**SS**	**F**	***p***	**SS**	**F**	***p***	**SS**	**F**	***p***
Model	74.83	11.40	0.0011	70.88	19.65	0.0001	2074.27	23.68	<0.0001	2208.54	28.89	<0.0001	919.51	7.98	0.0042
Significant				Significant			Significant			Significant			Significant		
A	42.23	19.30	0.0011	51.56	42.89	<0.0001	2037.77	69.80	<0.0001	2206.47	86.59	<0.0001	760.89	19.81	0.0010
B	31.44	14.37	0.0030	0.0084	0.007	0.9347	28.05	0.96	0.6469	0.053	0.002	0.9645	12.68	0.33	0.5775
C	1.16	0.53	0.4827	19.31	16.06	0.0021	8.45	0.29	0.6089	2.01	0.079	0.7840	145.95	3.80	0.0772
Lack of fit	15.28	0.39	0.8705	14.09	12.29	0.0775	312.26	7.81	0.1186	250.27	1.84	0.3996	360.51	1.29	0.5097
Not significant				Not significant			Not significant			Not significant			Not significant		

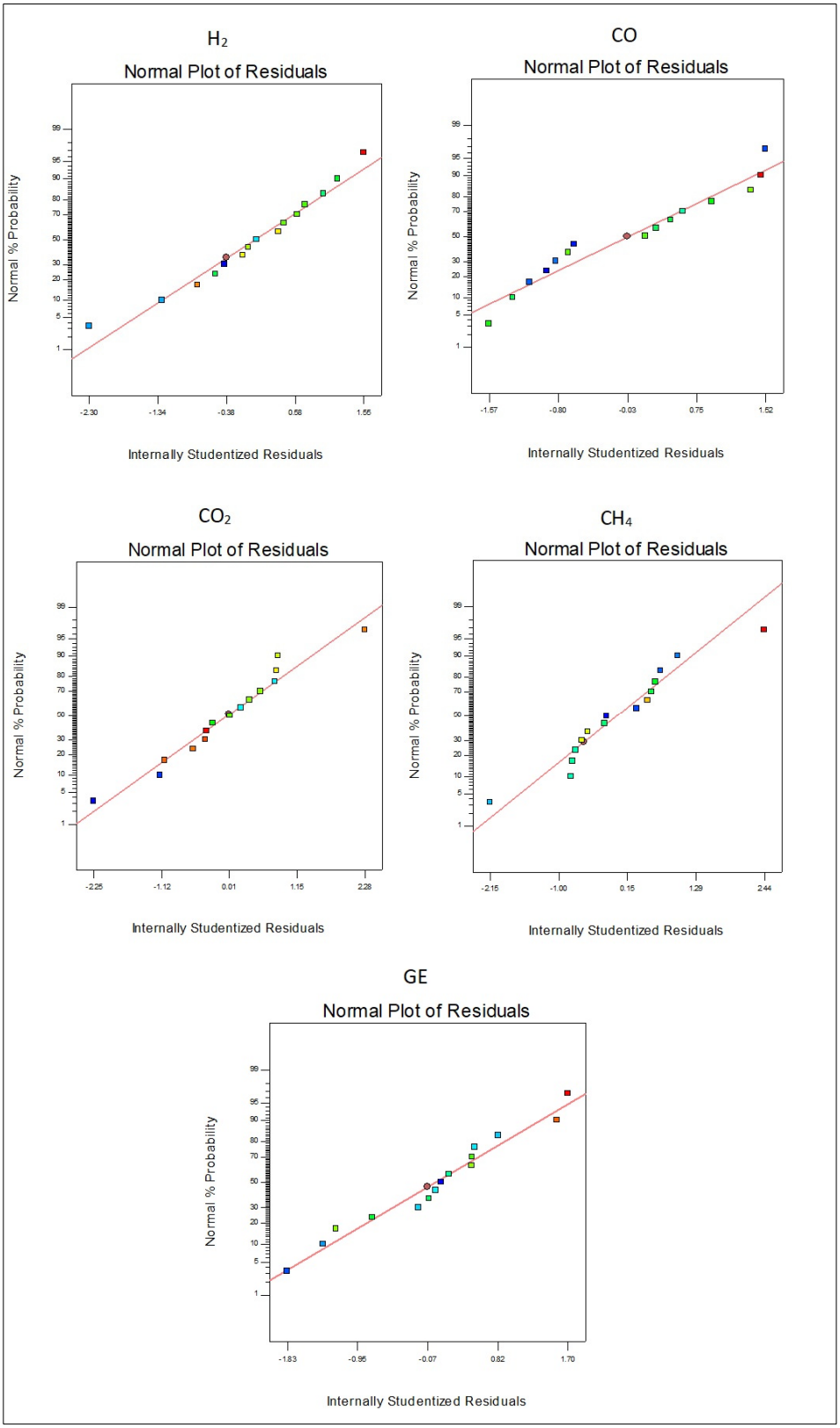

Figure 8. Normal probability plot of residuals.

Table 6. Model equations for response variables.

Response Variables (%)	Final Equations in Terms of Coded Factors	R^2	R^2adj	R^2pred
H_2	4.93 + 2.30A − 1.98B − 0.38C	0.7566	0.6902	0.6004
CO	3.61–2.54A + 0.032B − 1.55C	0.8428	0.7999	0.6784
CO_2	62.62–15.96A + 1.87B + 1.03C	0.8659	0.8294	0.7221
CH_4	28.63 + 16.61A + 0.081B + 0.50C	0.8874	0.8567	0.7733
GE	32.29 + 9.75A − 1.26B + 4.27C	0.6852	0.5994	0.4653

All adequacy indicators (R^2, adjusted R^2 and predicted R^2) are reasonably arranged and demonstrate a significant relationship. The coefficient of determination (R^2) should have a value of at least 0.6 to display the consistency and efficiency of the model accurately. According to Samiee-Zafarghandi [50], values of R^2 approaching 1 indicate good fitness of the model for experimental data. Furthermore, the divergences between adjusted coefficients of determination (R^2adj) and predicted coefficients of determination (R^2pred) were less than 0.2, which denotes reasonable accordance between them [50]. The values predicted by the model and the experimental data are displayed in Figure 9, suggesting a satisfactory agreement between them. Therefore, considering the range of experimental conditions investigated in this research, the RSM is a good tool to predict the results obtained from supercritical water gasification of biomasses.

3.4. The Effect of Variables on Gasification Products and Performance

3.4.1. The Effect of Variables on H_2 and CO Production

Figure 10 shows three-dimensional H_2 and CO production graphs when two variables change while the other is constant. The impact of biomass concentration, time and temperature variables on H_2 and CO content is exhibited in Figure 10a–f, respectively.

It is possible to notice in Figure 10c that at 25% of biomass loading, the H_2 content increased considerably with the rise in temperature from 400 to 500 °C, while CO production was reduced, which is in agreement with the results presented by previous studies [26,27,55]. Conforming to the Le Chatelier principle, the steam-reforming endothermic reactions, related to the H_2 production, are favored by higher reaction temperatures [56]. Furthermore, the weak exothermic nature of the water–gas shift reaction, an important route of H_2 production, becomes dominant with the increase in temperature. CO and water vapor act as reagents in a water–gas shift reaction, Hence, more H_2 is produced, and the content of CO reduces. CO is also consumed through exothermic methanation reaction as temperature indicating that kinetic effects were more dominant than thermodynamic effects within the temperature range used in this work [22,52,55].

Figure 10b shows a slight decrease in H_2 yield with time increments from 20 to 60 min during the reaction at 450 °C. Okolie [24] realized that the H_2 production from SCWG of soybean straw, at 500 °C, was elevated at 15 min, followed by a decline at 60 min. Other studies show that the concentration of H_2 was not modified substantially with the increase in time [57]. The divergent trend in these results can be attributed to the relation of time with other process variables, such as temperature. Researchers have reported that low temperatures (<500 °C) and long residence times do not favor H_2 formation [58,59]. From Figure 10e, it is possible to notice that increasing residence time reduces CO concentration in the gas. According to the literature, longer residence times favor hydrogenation and methanation reactions by consuming CO and H_2 to form CH_4. Thus, decreasing the H_2 and CO contents. Indeed, this is proven by studies that describe the higher H_2 and lower CO yields at higher temperatures (700–800 °C) and lower residence times (16–20 min) [22,27].

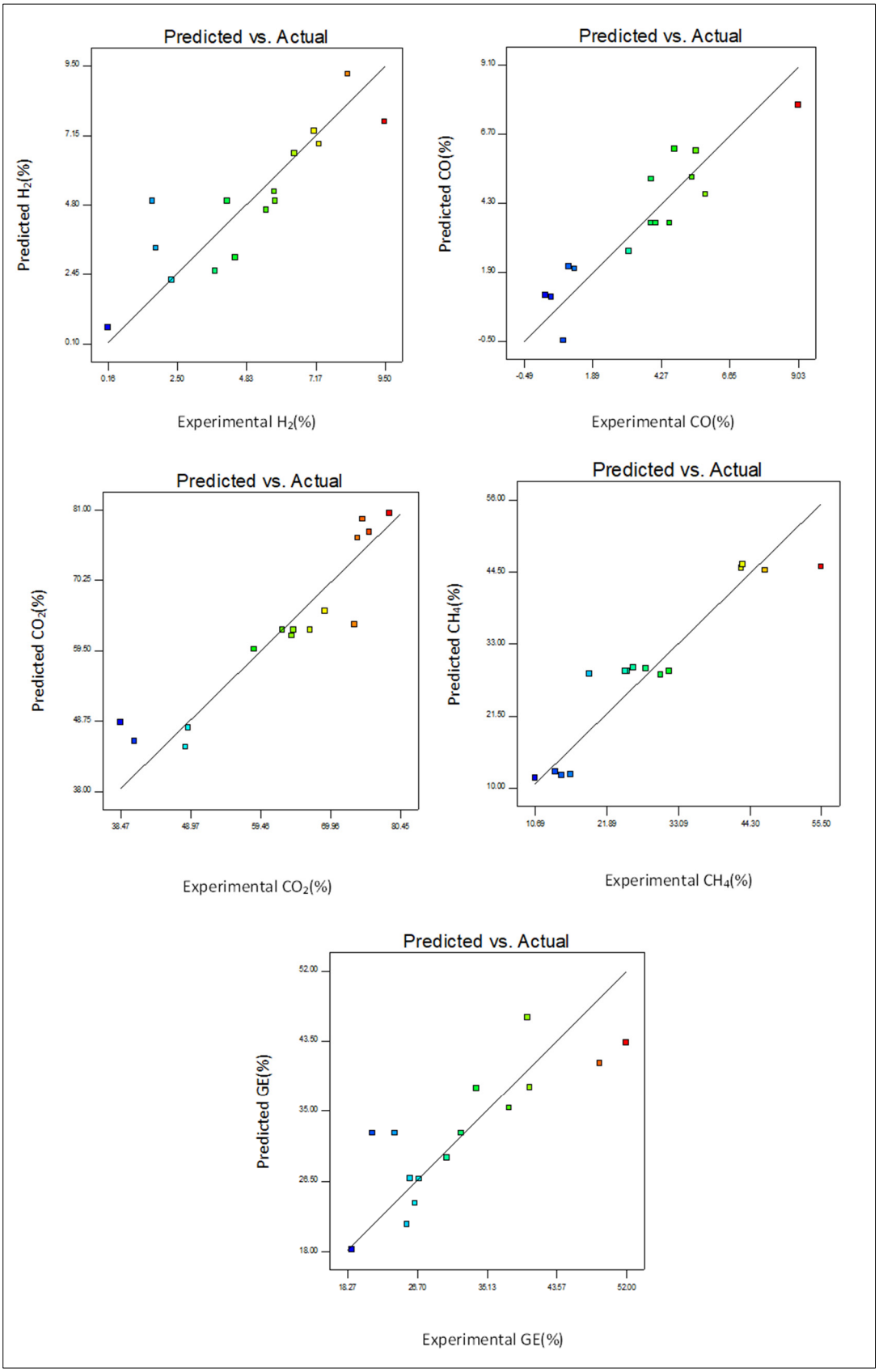

Figure 9. Predicted vs. actual response variables values.

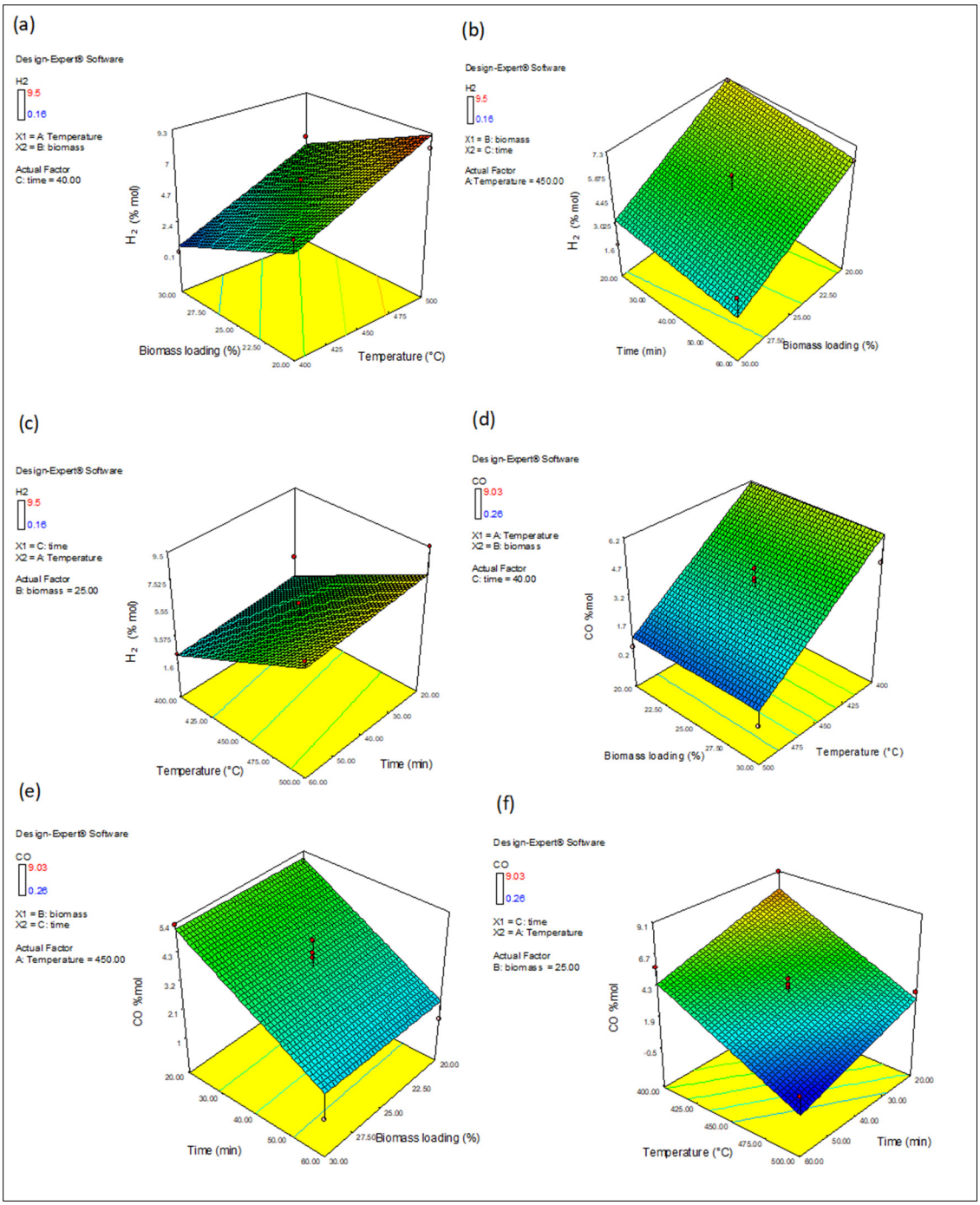

Figure 10. Three-dimensional response surface plots of interaction effects of variables on gas composition: H_2 (**a**–**c**) and CO (**d**–**f**) yields.

From Figure 10a it is evident that the content of H_2 decreased with the increase of biomass concentration from 20 wt% to 30 wt% at 40 min. This conclusion is presented by many authors [52,60]. A slight decrease in CO formation (Figure 10d) is due to increasing biomass loading. A similar trend was obtained by Nanda et al. [55]. Hydrolysis, steam reforming and water–gas shift reactions are limited in greater biomass loading, thus causing a reduction in H_2 and CO yield. High feed loading has a similarly lower water amount. In the steam reforming reaction, a high amount of water is desirable to react with hydrocarbons to produce H_2 and CO as the end products. To attain large hydrogen production, more water molecules at low feed concentrations should be provided [50,55].

3.4.2. The Effect of Variables on CO_2 and CH_4 Production

Figure 11 presents the three-dimensional response surface plots of the interaction effects of variables on CO_2 and CH_4 production.

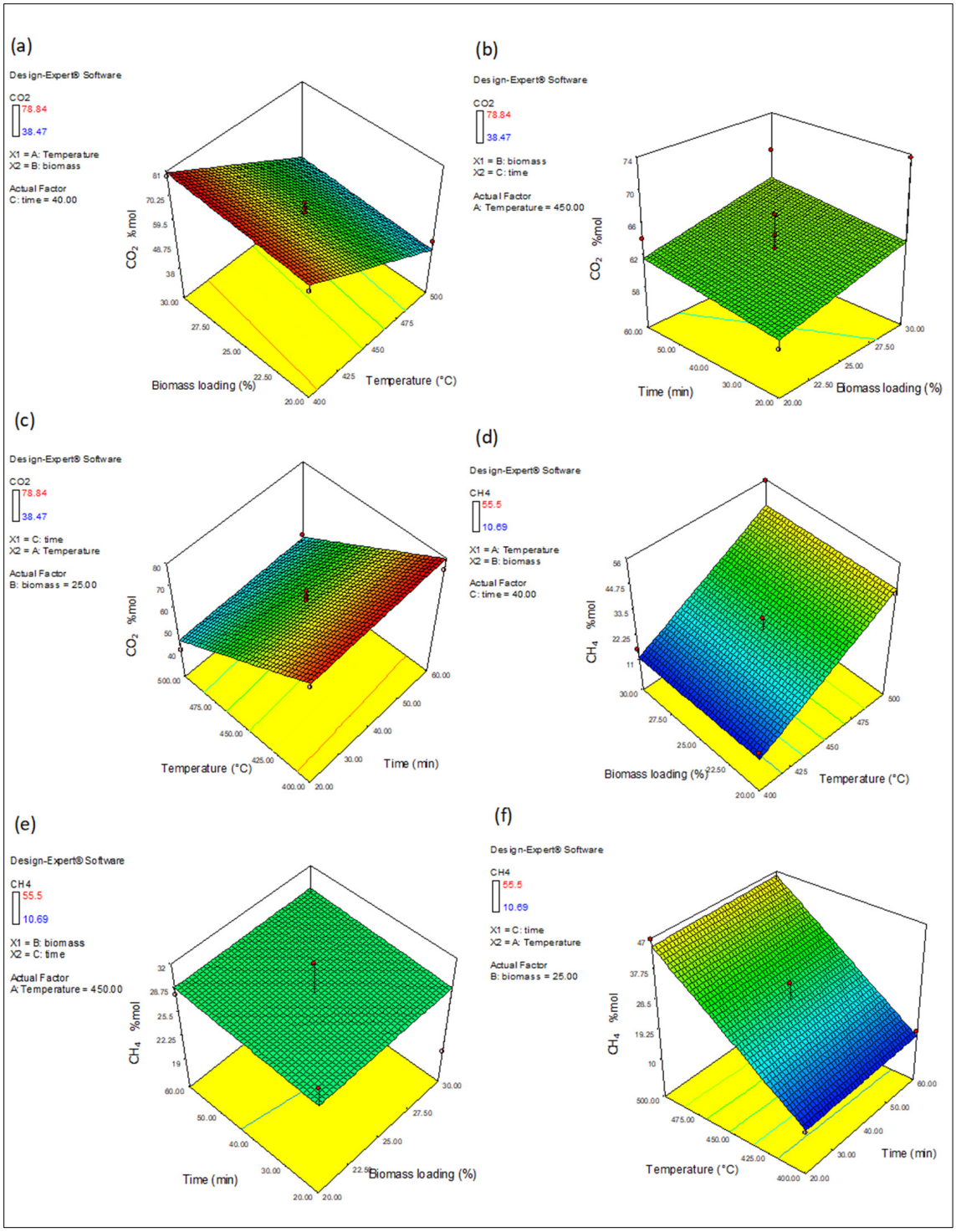

Figure 11. Three-dimensional response surface graphs of interaction effects of variables on gas composition: CO_2 (**a**–**c**) and CH_4 (**d**–**f**) yields.

As Figure 11c depicts, the CO_2 yield decreased with temperature increase. The same tendency was noticed by Wang et al. [61] and Ruya et al. [62] in their biomass SCWG experiments. According to these authors, the CO_2 predominance at low temperatures is a

consequence of the decarboxylation reactions of organic acids under this condition. With the increase in temperature, water becomes a potent oxidizing agent, favoring free radical reactions, which cause a reduction in CO_2 fraction in the gaseous product.

Additionally, at higher temperatures, hydrogen and methane production rates are higher than CO_2 [63]. Figure 11f shows that the temperature increase produced a divergent effect in CH_4 content. As the temperature rises, the methanation of CO_2 and CO and water–gas shift reactions are favored, increasing hydrogen and methane contents in the product gas [63]. Even though methanation is an exothermic process, the temperature used in this presented study was not deemed high enough to negatively impact this reaction.

The influence of time on CO_2 and CH_4 production, exhibited in Figure 11b,e, respectively, was insignificant. The increase in residence time, from 20 to 60 min, produced slight increments in CO_2 content. Similar results have been found in the literature [24,55,64]. According to Okolie [48], the CO_2 content is greater in the gas product as time increases as it is the main product of the water–gas shift reaction. At 20 wt% of biomass loading and 450 °C, the residence time increase did not produce great changes in CH_4 yields. However, at 30 w% of biomass loading, it was possible to observe that the higher the residence time higher the CH_4 yield. Cao et al. [27] and Amrullah and Matsumura [49] presented similar results in their studies. For the authors, the methanation reaction is favored at long residence times and higher biomass loading.

As presented in Figure 11a,d, with the increment in biomass loading from 20 to 30 wt%, slight changes were observed in CO_2 and CH_4 yields. At 400 °C and 40 min, a slight increase in CO_2 content was noticed, from 74.1 to 78.8 mol%. On the contrary, at 500 °C, the rise in biomass loading originated a decrease from 48.3 to 38.5 mol%. This result agrees with the information presented by Nanda et al. [64]. According to the researchers, reforming reactions are not favored at high biomass loading concentrations, reducing the H_2 and CO_2 yields. In spite of this, the smaller gas products of reforming reactions are compensated by the methanation of CO_2 that becomes considerable at large biomass concentrations. It was also observed that the rising biomass loading slightly favors the CH_4 yield. Demirel, Erkey and Ayas [52] noticed in their study that the CH_4 yield increased somewhat with an increase in biomass loading from 2.5% to 5%. Nanda et al. [64] also reported increments in CH_4 yield when the biomass loading was increased up to 35 wt%. Methanation and hydrogenation reactions are promoted at high biomass concentrations. Thus, more CH_4 is produced [55].

3.4.3. The Effect of Variables on GE, CGE and HGE

The influence of variables on gasification efficiency is shown in Figure 12. As shown in Figure 12b,c, the higher the process temperature and time, the higher the GE. However, from Figure 12a, it is clear that the increase in biomass concentration reduced the GE value.

According to Cao et al. [27], the steam-reforming reactions are endothermic. Therefore, according to the Le Chatelier principle, gas production will be intensified at a higher temperature. The longer residence time favors gasification efficiency because it enhances the gaseous production by rising thermal cracking and water–gas shift reactions, increasing the hydrogen yield [22,27]. The heat and mass transference between char and water is reduced with the rise in feed loading. Thus, the steam reforming and gas shift reactions are limited, decreasing the gasification efficiency and yield [22,27].

Figure 13 shows the percentages of CGE and HGE for experimental gasification runs at different temperatures, residence times and biomass loading, respectively.

The impact of temperature was analyzed at 20% of biomass loading and time of 40 min, as exhibited in Figure 13a. The temperature rise from 400 to 500 °C resulted in the highest values of CGE (97.4%) and HGE (69.3%). The increase in the CGE and HGE with temperature agrees with the documented trends [52,65]. Amrullah [49] reported that the gasification reaction rate is accelerated with increasing temperature, improving process efficiencies. The considerable increase in HGE (from 24.0 to 69.3%), exhibited in Figure 13a), results from the high hydrogen and methane yields in the gas at 500 °C. Moreover, the

amount of hydrogen formed depends on the biomass composition and the water used as a reaction medium in supercritical gasification. The rise in CGE value is due to the large carbon conversion at lower biomass concentration (20%).

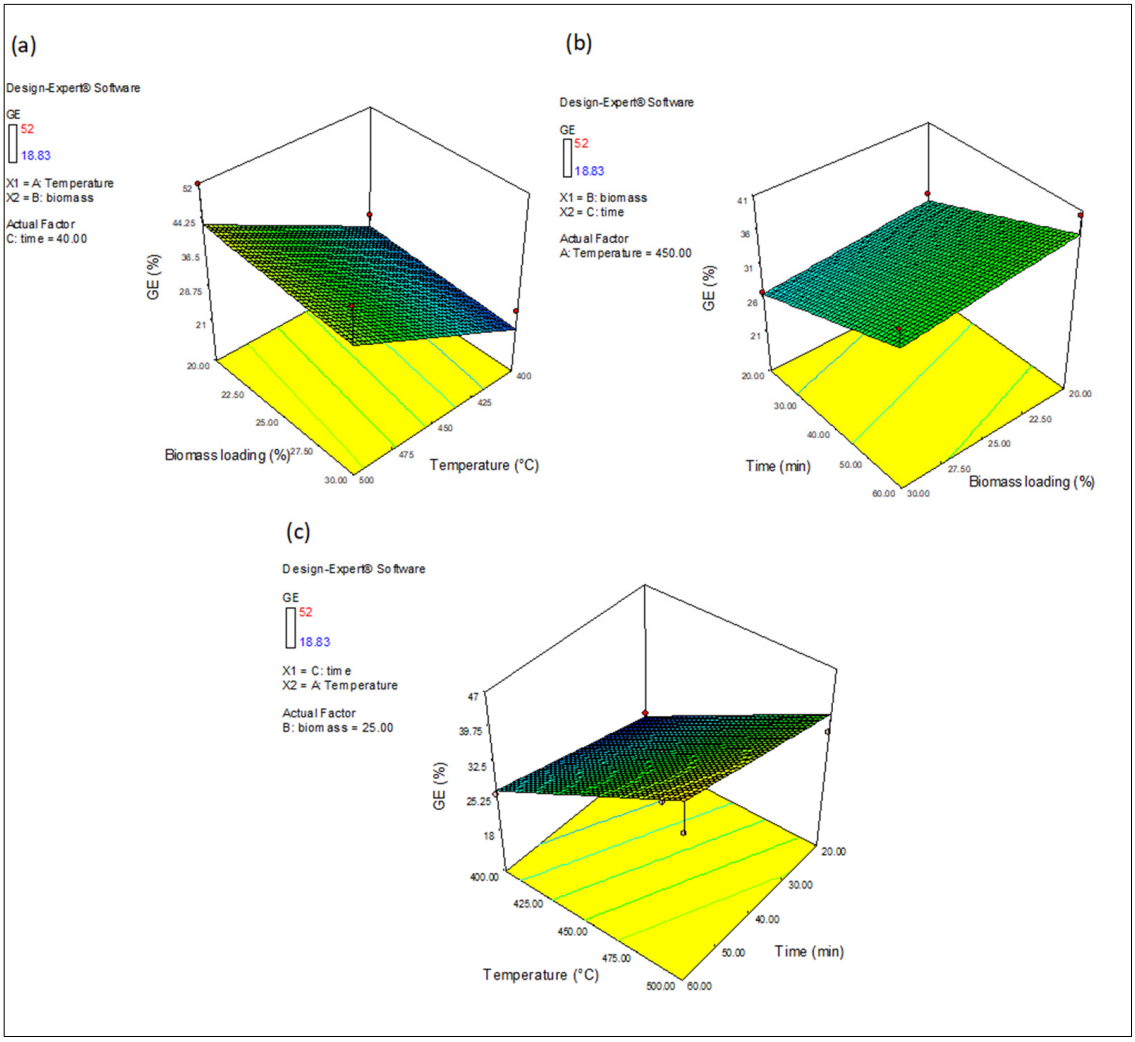

Figure 12. Three-dimensional response surface graphs of interaction effects of variables biomass concentration, temperature and time (**a**–**c**) on (GE).

The effect of variable feed loading on gasification efficiencies was studied at 500 °C and a time of 40 min. In Figure 13b, it was possible to see that the percentages of CGE and HGE were reduced when biomass loading was increased from 20 to 30%. However, the decrement in HGE value was more pronounced, changing from 45 to 69%. Probably, this occurred due to a noticeable decrease in H_2 content with increasing biomass loading. For Wang et al. [61], the increase in biomass concentration makes the complete interaction of biomass and supercritical water difficult, promoting the formation of complex components that were not easy to gasify.

The impact of time was investigated for gasification at 500 °C and biomass loading of 25 wt%. From Figure 13c, it is clear that the percentage of CGE considerably increased from 62 to 76%, with a rise in time from 20 to 60 min. On the contrary, the HGE value decreased from 52 to 47% in the same situation. According to Samiee-Zafarghand [50], increased CGE value with rising reaction time demonstrated rapid gas formation under supercritical water conditions. High reaction times are crucial for cracking reactions to produce gases [59]. However, longer residence times could favor hydrogenation and methanation reactions,

reducing CO and H_2 yields and producing more CH_4. Thus, the H_2 and CO yields, besides the HGE value, are decreased [24].

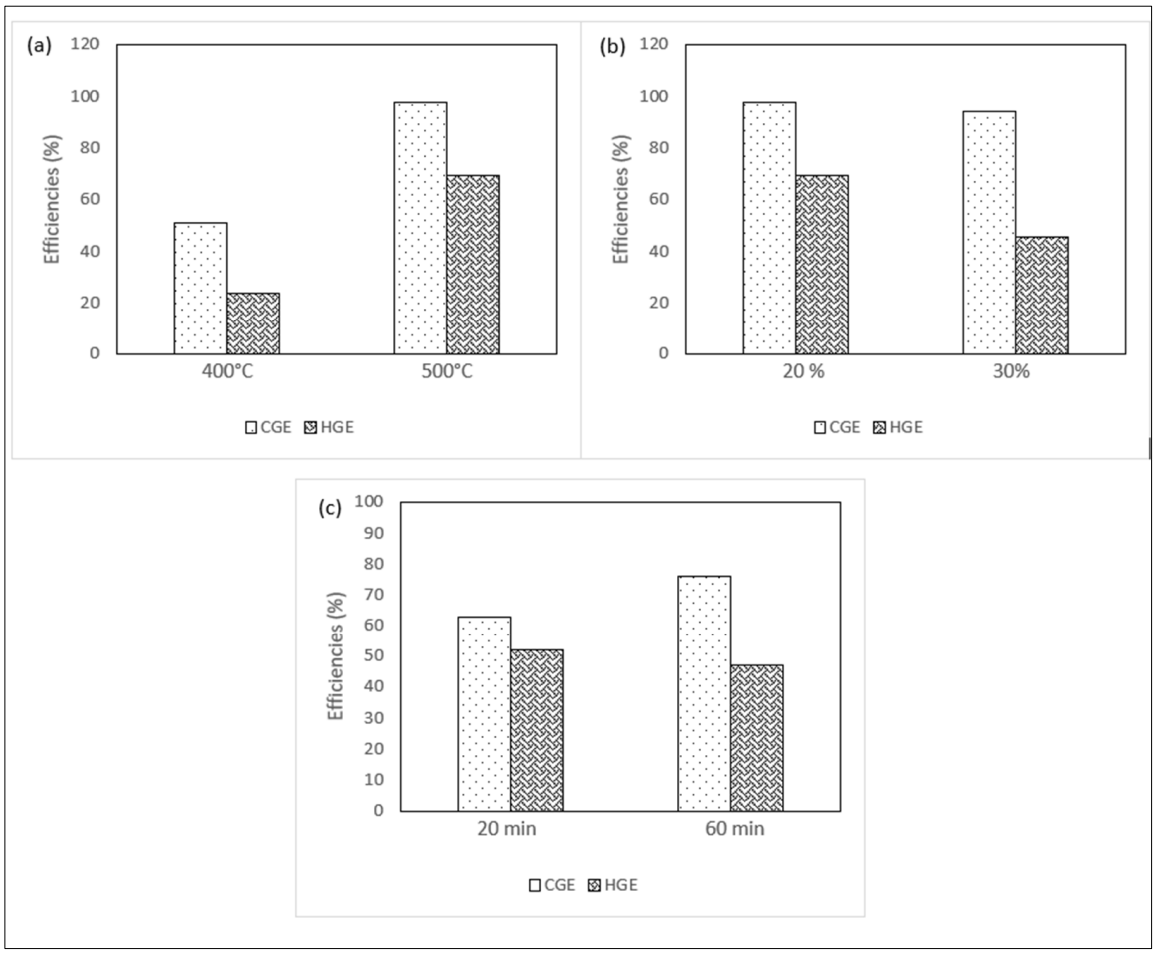

Figure 13. Effect of temperature (**a**), biomass loading (**b**) and time (**c**) on gasification efficiencies: CGE and HGE.

3.5. Optimization of the Model

The RSM involving a three-level Box–Behnken design was used in this research to investigate the relationship between the responses and the independent variables and to discover the optimum operation parameters to attain maximum H_2 content and GE value.

According to the results obtained in this study, the increase in temperature promoted H_2 production and gasification efficiencies. The gasification at 500 °C promoted a steam-reforming reaction, strongly related to increased gas yield and H_2 content. The reaction time impacts the gasification efficiency result from the higher gaseous production due to the enhancement of thermal cracking, water–gas shift reactions, and reduced H_2 yield. To reach higher H_2 contents in the gaseous mixture, modifying the experimental approach by reducing the residence time range or increasing temperature values could be necessary. Lastly, it was observed that the higher the biomass concentration, the lower the gasification efficiencies and H_2 yield.

Consequently, the constraints to optimize the responses are presented in Table 7, considering two different scenarios. Scenario 1 establishes temperature maximization, while scenario 2 minimizes residence time. The analysis of the prediction equation and surface plots provided by modelling in Design Expert software was essential to obtain the optimum conditions for the independent variables.

Table 7. Constraints to optimize the response.

Name	Scenario 1 Goal	Scenario 2 Goal	Lower Limit	Upper Limit
A—Temperature (°C)	maximize	in range	400	500
B—Biomass loading (wt%)	minimize	minimize	20	30
C—Time (min)	in range	minimize	20	60
H_2 (mol%)	maximize	maximize	0.2	9.5
GE (%)	maximize	maximize	18.8	52.0

The best conditions of the input parameters, which resulted in the maximum H_2 content and gasification efficiency (GE), are presented in Figure 14.

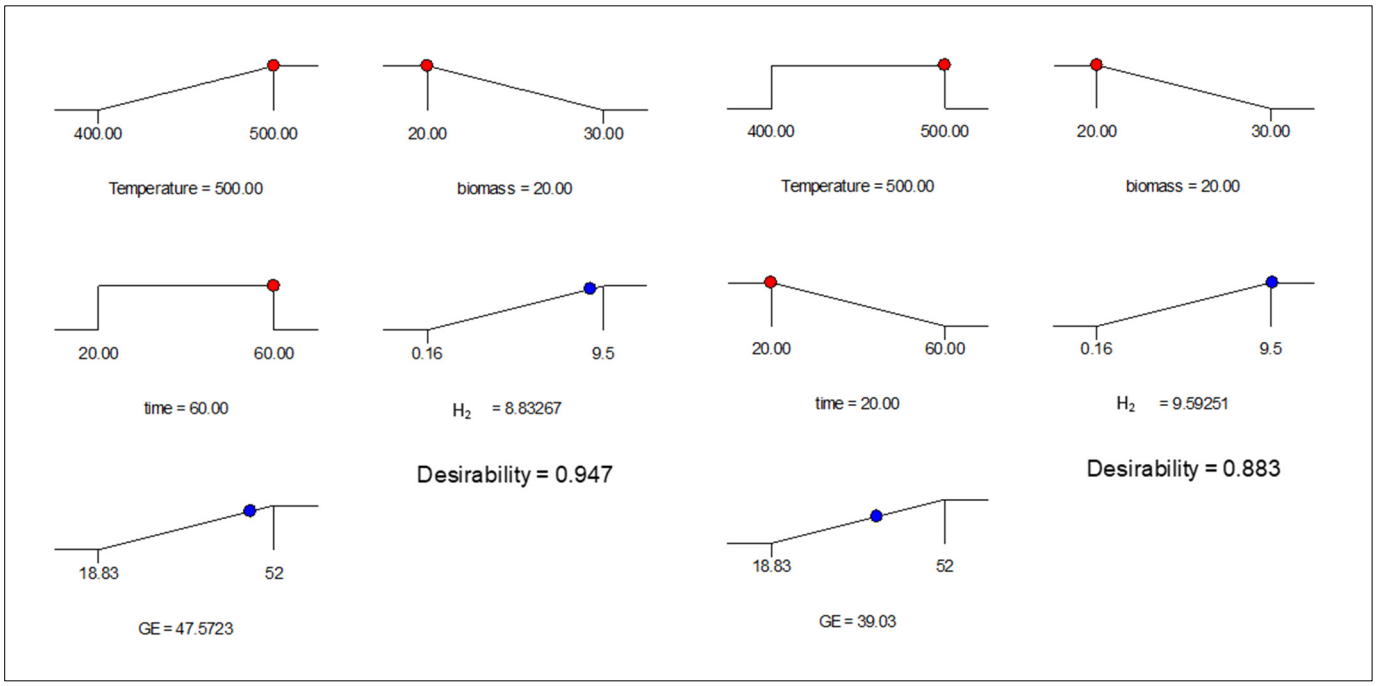

Figure 14. Ramps represent the best variables conditions for scenarios 1 and 2.

Under the established conditions for scenario 1, the supercritical water gasification of coconut shell provided an H_2 yield of 8.8 mol% and a GE of 47.6%. Considering scenario 2, more hydrogen (9.6%) could be produced. However, the gasification efficiency would be lower (39.0%).

The desirability data represents how accurate the response value is concerning the target. This value usually changes from 0 to 1 [50,66]. We have found a desirability data of 0.947, which shows that the optimization condition is better established under the condition presented for scenario 1.

To check the validity of this experimental model, it is desirable to perform a new experimental run under the optimum gasification conditions (500 °C, 60 min and 20 wt% of biomass loading). Moreover, catalysts can be a good alternative to reduce rough supercritical water gasification conditions, promoting higher hydrogen yields and process efficiency and declining tar and char production.

The ability of nickel nanoparticles to enhance gas production and gasification efficiency is one of the crucial aims for using them as active components for fuel generation from SCWG of biomass [67]. Therefore, the next section discusses the effect of this catalyst on efficiencies and gas composition from supercritical water gasification of impregnated samples.

3.6. Effect of Nickel Nanocatalyst on Supercritical Water Gasification

3.6.1. Effect of Nickel Nanocatalyst on the Gas Composition

This section evaluates the effects of nickel nanocatalyst impregnation on syngas composition and gasification efficiencies. Therefore, catalytic SCWG of coconut shell was carried out through 15 runs under the same experimental conditions of temperature, residence time and biomass loading previously used. The design and the attained results are presented in Table 8.

Table 8. Gaseous product characteristics for supercritical water gasification of impregnated coconut shell samples.

				Response Variables				
Run	**A—Temperature (°C)**	**B—Residence Time (min)**	**C—Biomass Loading (wt%)**	**H_2**	**CO**	**CO_2**	**CH_4**	**GE**
1	500	40	20	8.6	3.0	43.7	44.8	54.8
2	400	40	20	4.5	7.1	71.8	16.5	41.4
3	400	60	25	3.3	9.7	59.9	27.0	45.4
4	450	40	25	7.8	12.6	52.8	26.9	29.4
5	450	20	30	4.6	12.4	55.8	27.2	31.5
6	450	20	20	17.2	15.7	48.1	18.9	33.7
7	450	60	30	3.9	6.0	49.1	40.9	42.8
8	500	20	25	13.0	7.7	42.8	36.7	49.3
9	400	20	25	4.6	14.5	56.1	24.8	29.4
10	450	40	25	4.2	13.0	54.8	27.9	48.0
11	450	60	20	7.6	12.0	42.0	38.4	44.5
12	400	40	30	5.6	11.9	59.5	22.9	40.5
13	500	40	30	5.8	8.7	48.6	36.9	51.2
14	500	60	25	8.0	1.02	48.4	42.6	58.6
15	450	40	25	6.9	12.5	53.2	27.4	37.4

According to the data shown in Table 8, during the catalytic supercritical water gasification process, as observed in the non-catalytic process, CO_2 was also produced as a dominant gas in run 2, with a maximum value of 71.8 mol% at 400 °C, with the lowest feed concentration (20 wt%) in 40 min. However, the content is slightly lower than that realized in the gasification under the same experimental conditions without a catalyst (74.1 mol%). Comparing the results in Table 4, all percentages of CO_2 in the product gas reduced after the catalyst addition. Borges et al. [26] have found a similar trend in their study of the catalytic gasification process. According to the authors, it can be attributed to the capacity of a nickel catalyst to promote the methanation of CO_2 in longer residence times.

In Table 8 for run 1, that the maximum CH_4 content produced in the catalytic process was 44.8 mol%, obtained at 500 °C, 40 min and in the minimum biomass loading (20 wt%). Under the same operational condition, a similar amount of 43.0 mol% of CH_4 was produced without a catalyst. However, the CH_4 yields were higher for almost all experimental runs when a nickel catalyst was used. For example, at 450 °C, 60 min and 30 wt% of biomass loading, 26 mol% of CH_4 was produced in the non-catalytic process. Under the same conditions, 40.9 mol% of CH_4 was obtained in the catalytic process. The improvement in CH_4 content by nickel catalyst supercritical water gasification has been reported in the literature [18,20]. According to the authors, it occurs due to the action of nickel on the methanation reaction, promoting a higher selectivity towards CH_4.

Concerning H_2 and CO production, it is clear from Table 8 that the maximum H_2 and CO production was 17.2 mol% and 15.7 mol%, respectively. These yields were produced at 450 °C with 20 wt% of biomass during 20 min. Compared with the results achieved in the non-catalytic process for the same conditions, the catalyst presence contributed to the increase in the content of these gaseous components from 7.1 and 3.9 mol% for H_2 and CO, respectively. Said et al. [34] described in their study that the presence of nickel involved

a noticeable rise in the CO and H_2 production at 500 °C for wood-impregnated samples. According to Nanda et al. [20], nickel is an effective hydrogenation catalyst, decomposing biomass primarily to CO and H_2. The generation of soluble organics in the initial stage of biomass degradation undergoes cracking reactions promoted at the nickel surface. Their interaction with water results in larger yields of H_2 [19].

The highest GE value (58.6%) was found at 500 °C with 25% of biomass during 60 min. When the same operational condition was employed in the non-catalytic gasification, a GE of 40.1% was obtained. The gasification efficiency is directly associated with gas yields. In their study, Zhang et al. [68] observed that the nickel catalyst produced significant gas contents compared with the SCWG process without a catalyst. Experiments developed by Said et al. [34] confirmed the promotion of gas yield between 500 and 600 °C as a result of the activation of in-site nickel nanoparticles during SCWG. The impregnation of biomass with nickel favors higher gas yield production at higher temperatures. Ni^{2+} is transformed into a metallic form under this condition, accelerating C–C bond breakage and promoting the degradation of the biomass [18].

More details about the influence of process variables on catalytic supercritical water gasification, products yields, gas composition and process efficiencies are provided in the next section.

Impact of the Process Variables on the Catalytic SCWG

The product yielded from the SCWG of control and impregnated coconut shell samples are shown in Table 9. From these data, it was possible to comprehend how experimental conditions affect the routes of gas, liquid and solid production.

Table 9. Solid, liquid and gas yields from SCWG of control and impregnated biomass.

Variables			Control Sample			Impregnated Sample		
Biomass Loading (%)	**Temperature (°C)**	**Residence Time (min)**	**Solid (wt%)**	**Liquid (wt%)**	**Gas (wt%)**	**Solid (wt%)**	**Liquid (wt%)**	**Gas (wt%)**
20	400	40	12.4	61.1	26.5	11.9	46.7	41.4
	500	40	11.9	36.1	52.0	9.2	36.0	54.7
	450	20	10.1	59.6	30.3	9.1	57.2	33.7
	450	60	9.8	49.9	40.4	9.6	45.9	44.5
25	450	40	14.7	61.3	24.0	12.0	58.6	29.4
	450	40	12.5	66.1	21.3	11.5	40.5	48.0
	450	40	9.9	58.1	32.0	9.6	53.0	37.4
	400	20	15.8	65.4	18.8	12.5	58.1	29.4
	400	60	12.5	61.6	25.9	7.5	47.1	45.4
	500	20	15.7	50.4	33.9	13.3	37.4	49.3
	500	60	12.3	47.6	40.1	11.1	30.3	58.6
30	400	40	13.7	60.8	25.5	13.3	46.2	40.5
	500	40	13.5	37.7	48.8	13.0	35.2	51.8
	450	20	13.9	59.1	26.9	12.6	55.9	31.5
	450	60	14.9	47.2	37.9	12.1	45.1	42.8

At the same biomass loading and residence time, the change in temperature values from 400 to 500 °C increased the gas yields and decreased the solid and liquid amounts for both samples. Comparable results were found in the literature [24,26,64]. According to Nanda et al. [20], the increment in gas yields at higher temperatures is due to improved reactions such as water–gas shift and steam reforming under the supercritical water condition. A similar trend occurred when residence time values increased from 20 to 60 min. Longer reaction times favor the occurrence of secondary reactions, causing the breakdown of high molecular weight species to gases [20].

With the rise in biomass concentration from 20 to 30 wt%, it was observed that the solid yield was slightly increased. However, the liquid yield was lower when 30 wt% of biomass loading was employed under the same condition. This occurred because higher

biomass concentration restricted some reactions such as hydrolysis, reducing liquid yields and enhancing the solid content [20].

Analyzing all data in Table 9 for control and impregnated samples, it was possible to notice reductions in the solid and liquid yields. According to Borges et al. [26], the nickel catalyst inhibited the polymerization of the carbon, decreasing tar and/or char formation. However, it should also be highlighted that the larger yield of liquid products (reaching up to 58% in the catalytic process) is the cause of the medium of gasification being water, which also acts as the solvent [24,64]. The lowest production of solid residue (7.5%) and the highest gas formation (45.4%) was attained from the runs using catalyst at 400 °C, 60 min and 25 wt% of biomass loading. It was also observed that the highest gas content and the lowest liquid yield, 58.59 and 30.31%, respectively, were found for the catalytic process at 500 °C, 60 min and 25 wt% of biomass loading. The results presented in Table 9 show that the amount of gas produced is higher in the catalytic process for all experimental conditions. This observation agrees with recent literature reports [18–20,68], where the authors describe that the gas yield for the nickel-impregnated samples was much higher than the control samples. Accordingly, these results show the catalyst's ability to degrade complex intermediates, such as tar components, into gases.

According to the experimental design procedure used in this study, 15 tests were performed for control and impregnated samples and 3 reproductions of the central point (450 °C, 40 min and 25% wt) were executed to analyze the experimental error. For control samples, the calculated amounts of solid, liquid and gas were 12.37 ± 1.96 (wt%), 61.83 ± 3.28 (wt%) and 25.76 ± 4.54 (wt%). Regarding impregnated sample, 11.03 ± 1.03 (wt%), 50.7 ± 7.56 (wt%) and 38.26 ± 7.61 (wt%) of solid, liquid and gas were obtained, respectively. The highest calculated standard error of 7.61 can be considered a permissible error since some experimental errors occurred during product collection, which could originate some losses in the mass balance. Information about the impact of process variables on process efficiency and gas composition from catalytic supercritical water gasification is discussed in the next section.

Temperature

Figure 15 presents the trend of gas composition and efficiencies (CGE and HGE) concerning catalytic supercritical water gasification at different temperatures (400 and 500 °C), 20 wt% of biomass loading and residence time of 40 min.

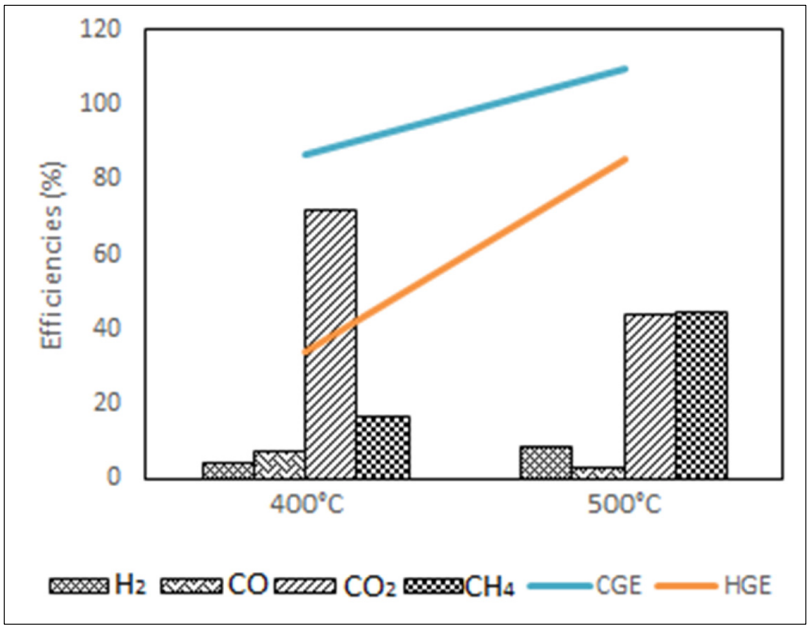

Figure 15. Influence of temperature on gas composition and process efficiencies.

The higher temperature (500 °C) contributed to the H_2 increment (from 4.5 to 8.6 mol%) and CH_4 yields (from 16.5 to 44.8 mol%), and improvements in CGE and HGE values, reaching up to 109 and 85%, respectively. The CO and CO_2 yields were reduced with the temperature increase, from 7.1 and 71.8 mol% to 3.0 and 43.7 mol%, respectively. A similar trend was observed in the non-catalytic process.

As shown in Table 4, at 500 °C, 20 wt% of biomass loading and residence time of 40 min, 8.3 mol% of H_2, 0.5 mol% of CO, 48.3% mol of CO_2 and 43.0 mol% of CH_4 were obtained in the non-catalytic process. For the gasification efficiencies, CGE of 97.4% and HGE of 69.3% were found. Compared with the results obtained for the catalytic process, the presence of the nickel nanocatalyst enhanced H_2, CH_4 and CO yields and gasification efficiencies. However, the amount of CO_2 was slightly reduced.

Rises in H_2, CH_4 and CO yields and gasification efficiencies have been reported in the literature for nickel impregnation at high temperatures [18,20]. According to the authors, nickel acts on the decomposition of biomass to CO and H_2, which further react to give CH_4 via a methanation reaction. In their study about the catalytic gasification process, Borges et al. [26] found a reduction trend for CO_2 yield. According to the authors, it can be attributed to the capacity of a nickel catalyst to promote the methanation of CO_2 at longer residence times.

The CGE value for the impregnated sample is usually greater than the obtained for the control sample due to the capacity of the nickel catalyst to degrade the complex components formed during the gasification [18]. Moreover, according to Chen et al. [22], CGE values higher than 100% indicated that complete gasification was achieved in the catalyst's presence. The rise in HGE results from the larger H_2 and CH_4 contents under the catalytic condition.

Biomass Loading

The effect of changing biomass loading values from 20 to 30 wt% on gaseous products and process efficiencies was studied at 500 °C and 40 min. The results are presented in Figure 16.

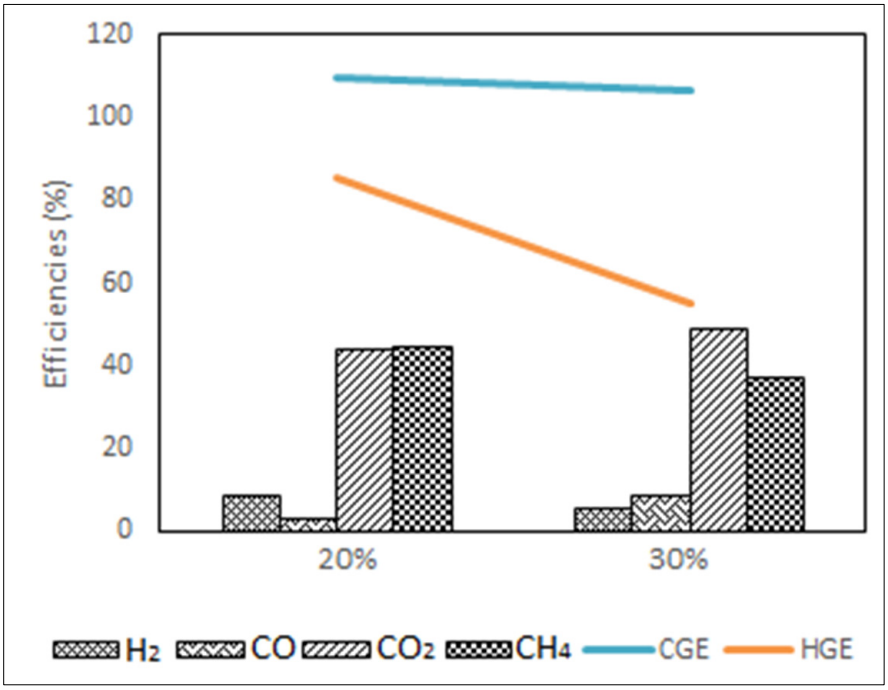

Figure 16. Influence of biomass loading on gas composition and process efficiencies.

The rise in biomass loading led to a reduction in H_2 and CH_4 yields and gasification efficiencies. The decrease in H_2 content, from 8.6 mol% to 5.8 mol%, with an increase in

biomass loading was also observed for the gasification without a catalyst. A reduction in CH_4 yield was noticed from 44.8 mol% to 36.9 mol%, which represented an opposite trend in comparison with the non-catalytic process. This behavior suggests that the in situ presence of the nano nickel catalyst is not favorable for hydrogen and methane production for catalytic supercritical gasification with high biomass loading. This result agrees with that reported by Resende and Savage [69], where it was observed that 33.3% of biomass loading gave the most significant decrease in H_2 and CH_4 yields in the presence of nickel catalyst. However, better results were obtained when 5% of biomass loading was employed. It is possible to infer that nickel catalyst gave higher activity for water–gas shift and methanation reactions at 20 wt% of biomass loading.

The contents of CO and CO_2 were favored with increasing biomass concentration in the catalytic process. The CO_2 yield rose slightly, from 43.7 to 48.7 mol%. The increase of CO was more pronounced, from 3.0 to 8.7 mol%. The results in Table 4 for the non-catalytic process under the same experimental condition showed an opposite trend. Increases in CO_2 and decreases in CO contents due to increased biomass loading in the catalytic supercritical water gasification with nickel were reported by Huang et al. and Pairojpiriyakul et al. [17,70]. As discussed previously, for the non-catalytic process, the reforming, water–gas shift and steam reforming reactions related to the production of CO and CO_2 are retarded primarily at high feed concentrations. From our experiments, it can be inferred that nickel deposition onto biomass surfaces can accelerate these reactions. The product gas yields from these reactions improved remarkably.

As found in the non-catalytic process, increased CGE and HGE values were not favored by increased biomass loading. However, under the same operational condition (500 °C, 40 min and 30% of biomass loading without a catalyst), lower CGE and HGE values (93.9 and 45.4%, respectively) than those found in the catalytic process (CGE of 106.6% and HGE of 54.9%) were observed. The CGE value higher than 100% indicates the complete gasification of carbon in the presence of nickel. These results also illustrate that the nickel catalyst had good activity on supercritical water gasification of biomass for both concentrations (20 and 30%). Similar results were reported by Huang et al. [17].

Reaction Time

Figure 17 shows how the gas composition and gas efficiencies are influenced by changing the residence time from 20 to 60 min, during catalytic supercritical water gasification at 500 °C and 25 wt% of biomass loading.

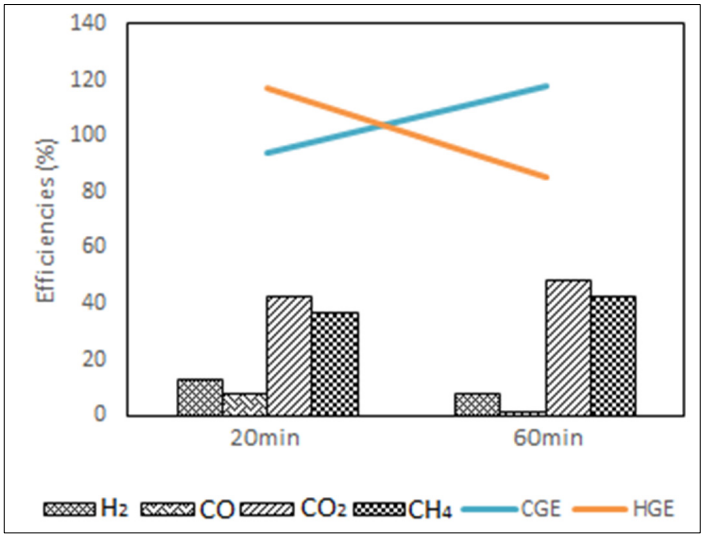

Figure 17. Influence of residence time on gas composition and process efficiencies.

Analyzing Figure 17, it is evident that the higher the residence time, the higher the CO_2 and CH_4 yields and CGE value. The contents of CO_2 and CH_4 rose slightly from 43 to 48 mol% and from 37 to 43 mol%, respectively. Pairojpiriyakul et al. [70] reported a similar result. This trend is also according to that obtained for the non-catalytic process. Water–gas shift and methanation reactions are favored at longer residence times, promoting the production of CO_2 and CH_4, respectively. The increase in the CGE value up to 117.81% was sharper than those found in the non-catalytic process under the same experimental condition, i.e., 75.86%. The literature reports a similar trend for the SCWG of biomass using a nickel catalyst [17,20], showing that nickel-impregnated samples enhanced the degradation, resulting in greater gas content at larger temperatures and residence time.

The contents of H_2, CO and the HGE value reduced when the reaction time increased from 20 to 60 min. A decline in H_2 and CO yields was noticed, from 13.03 to 8.04 mol% and from 7.65 to 1.02 mol%. The same trend was observed for the process without a catalyst under the same operational condition. However, the H_2 and CO contents in the syngas were higher than those obtained for the non-catalytic supercritical water gasification at 500 °C, 25% of biomass loading and 20 min, (9.5 and 3.16 mol%, respectively), which suggests that the presence of nickel improves the methanation reaction. As previously presented for the process without a catalyst, a reduction in HGE value was noticed, from 116.91% to 85.62%. Despite this reduction, these values are much higher than those obtained for the non-catalytic process under the same experimental conditions. A higher residence time benefits hydrogenation and methanation reactions by producing CH_4. This way, the yields of H_2 and CO as well as the HGE value are reduced [24].

4. Conclusions

In this work, a sample of coconut shell biomass was impregnated with nickel catalyst to evaluate its performance in enhancing H_2 yield and supercritical water gasification efficiency. Control and impregnated samples were characterized by physicochemical analysis to confirm the resulting differences from the nickel presence. The results also confirmed that coconut shell is a good combustible source for more efficient energy products.

The samples were gasified using supercritical water under different experimental conditions to determine how the process variables and catalyst impregnation impact the gas composition and efficiency. The RSM using Box–Behnken approach was used to design the experiments. Regression models were obtained between the responses and the three independent variables. The effects of each variable on each component of produced gas (mol%) and gasification efficiency were indicated through ANOVA analysis. From this analysis, the significance of temperature in determining the composition of all gaseous products and process efficiency was clear. For H_2 content, biomass loading was also emphasized as a significant factor. The predicted values obtained by the models agreed with the experimental values. The results obtained under the non-catalytic condition showed that the H_2 yield and GE value were privileged at high temperatures, time and low biomass loading. The influence of variables on product yields was also evaluated, where it was noticed that the increment in temperature and time values produced a rise in the gas yields and a decrease in char and tar contents. However, more char was produced with the increase in biomass loading.

The experiments with impregnated biomass found that the maximum H_2 production was 17.2 mol% at 450 °C with 20 wt% of feed concentration for 20 min. This result confirmed that the impregnated nickel nanoparticles have the potential to catalyze hydrogen-forming reactions. The highest GE value (58.6%) was obtained at 500 °C with 25 wt% of biomass loading during 60 min, indicating the action of nickel nanocatalyst enhancing the gas yield. The highest CGE (109.4%) and HGE values (116.9%) were found in the catalytic process at 500 °C and 40 min, indicating that complete gasification was attained in the presence of the catalyst. The nickel nanocatalyst also enhanced the gas content and reduced the solid and liquid yields due to the catalyst's ability to degrade complex intermediates, such as tar components, into gases.

The findings from this study indicate that nickel catalyst impregnation into coconut shell biomass can be an attractive alternative for catalytic SCWG to produce H_2-rich syngas with higher efficiency. Complementary studies should be carried out to further the knowledge about this promising thermochemical conversion route involving different feedstocks. Still, the analysis of the effect of varying nickel concentrations and operational conditions on the process yield is currently going on to improve this technology.

Author Contributions: Conceptualization, M.M.M., G.A.L., G.J., S.A.B.V.d.M. and E.A.T.; methodology, M.M.M., G.A.L., G.J., J.A.O. and C.T.A.; writing—original draft preparation, M.M.M., G.A.L. and G.J.; writing—review and editing, M.M.M., G.A.L., S.A.B.V.d.M., E.A.T., D.M.d.S. and F.A.T.; supervision, G.A.L., G.J., C.T.A., E.A.T. and S.A.B.V.d.M. All authors have read and agreed to the published version of the manuscript.

Funding: This study was partly financially supported by Coordenação de Aperfeiçoamento de Pessoal de Nível Superior, Finance Code 001 (CAPES, Brazil) and Fundação de Amparo à Pesquisa do Estado da Bahia (FAPESB, Brazil), INCITERE Project, PIE0008/22.

Data Availability Statement: The authors confirm that the data supporting the findings of this study are available within the article.

Acknowledgments: This study was conducted at the School of Chemical Engineering at the University of Birmingham and the European Bioenergy Research Institute (EBRI) at Aston University. The authors would like to show great gratitude to the CAPES (Coordenação de Aperfeiçoamento de Pessoal de Nível Superior), FAPESB (Fundação de Amparo à Pesquisa do Estado da Bahia), Supercritical Fluids, Fuel Cell and Hydrogen Research laboratories at the University of Birmingham, as well as their colleagues that provided them with the opportunity to finish the project.

Conflicts of Interest: The authors declare no conflict of interest. The funders had no role in the design of the study; in the collection, analyses, or interpretation of data; in the writing of the manuscript; or in the decision to publish the results.

References

1. Ahmad, R.K.; Sulaiman, S.A.; Yusup, S.; Dol, S.S.; Inayat, M.; Umar, H.A. Exploring the potential of coconut shell biomass for charcoal production. *Ain Shams Eng. J.* **2021**, *13*, 101499. [CrossRef]
2. Azeta, O.; Ayeni, A.O.; Agboola, O.; Elehinafe, F.B. A review on the sustainable energy generation from the pyrolysis of coconut biomass. *Sci. Afr.* **2021**, *13*, e00909. [CrossRef]
3. Caballero, D.R.C.; Barraza, J.; Gunasekaran, S.; Roa-Espinosa, A.; Colina-Márquez, J.; Machuca-Martínez, F.; Hernández-Ramírez, A.; Vazquez-Rodriguez, S. Experimental data on the production and characterization of biochars derived from coconut-shell wastes obtained from the Colombian Pacific Coast at low temperature pyrolysis. *Data Brief* **2020**, *28*, 104855. [CrossRef]
4. Sarkar, J.K.; Wang, Q. Different Pyrolysis Process Conditions of South Asian Waste Coconut Shell and Characterization of Gas, Bio-Char, and Bio-Oil. *Energies* **2020**, *13*, 1970. [CrossRef]
5. Akolgo, G.A.; Awafo, E.A.; Essandoh, E.O.; Owusu, P.A.; Uba, F.; Adu-Poku, K.A. Assessment of the potential of charred briquettes of sawdust, rice and coconut husks: Using water boiling and user acceptability tests. *Sci. Afr.* **2021**, *12*, e00789. [CrossRef]
6. Inayat, M.; Sulaiman, S.A.; Kurnia, J.C. Catalytic co-gasification of coconut shells and oil palm fronds blends in the presence of cement, dolomite, and limestone: Parametric optimization via Box Behnken Design. *J. Energy Inst.* **2019**, *92*, 871–882. [CrossRef]
7. Menon, S.D.; Sampath, K.; Kaarthik, S.S. Feasibility studies of coconut shells biomass for downdraft gasification. *Mater. Today Proc.* **2021**, *44*, 3133–3137. [CrossRef]
8. Yahaya, A.Z.; Somalu, M.R.; Muchtar, A.; Sulaiman, S.A.; Daud, W.R.W. Effect of particle size and temperature on gasification performance of coconut and palm kernel shells in downdraft fixed-bed reactor. *Energy* **2019**, *175*, 931–940. [CrossRef]
9. Nanda, S.; Isen, J.; Dalai, A.K.; Kozinski, J.A. Gasification of fruit wastes and agro-food residues in supercritical water. *Energy Convers. Manag.* **2016**, *110*, 296–306. [CrossRef]
10. Wang, C.; Jin, H. Development of a Partitioning Kinetic Model of Biomass Gasification in Supercritical Water with a Fluidized Bed Reactor. *Ind. Eng. Chem. Res.* **2022**, *61*, 10058–10068. [CrossRef]
11. Wang, C.; Li, L.; Shi, J.; Jin, H. Biochar production by coconut shell gasification in supercritical water and evolution of its porous structure. *J. Anal. Appl. Pyrolysis* **2021**, *156*, 105151. [CrossRef]
12. Ciuta, S.; Tsiamis, D.; Castaldi, M.J. *Gasification of Waste Materials: Technologies for Generating Energy, Gas, and Chemicals from Municipal Solid Waste, Biomass, Nonrecycled Plastics, Sludges, and Wet Solid Wastes*; Academic Press: Cambridge, MA, USA, 2017.
13. Ibrahim, A.; Akilli, H. Supercritical water gasification of wastewater sludge for hydrogen production. *Int. J. Hydrog. Energy* **2019**, *44*, 10328–10349. [CrossRef]

14. Lee, C.S.; Conradie, A.V.; Lester, E. Review of supercritical water gasification with lignocellulosic real biomass as the feedstocks: Process parameters, biomass composition, catalyst development, reactor design and its challenges. *Chem. Eng. J.* **2021**, *415*, 128837. [CrossRef]
15. Azadi, P.; Farnood, R. Review of heterogeneous catalysts for sub- and supercritical water gasification of biomass and wastes. *Int. J. Hydrog. Energy* **2011**, *36*, 9529–9541. [CrossRef]
16. Richardson, Y.; Blin, J.; Volle, G.; Motuzas, J.; Julbe, A. In situ generation of Ni metal nanoparticles as catalyst for H2-rich syngas production from biomass gasification. *Appl. Catal. A Gen.* **2010**, *382*, 220–230. [CrossRef]
17. Huang, J.; Zhu, C.; Lian, X.; Feng, H.; Sun, J.; Wang, L.; Jin, H. Catalytic supercritical water gasification of glucose with in-situ generated nickel nanoparticles for hydrogen production. *Int. J. Hydrog. Energy* **2019**, *44*, 21020–21029. [CrossRef]
18. Kumar, A.; Reddy, S.N. In Situ Sub-and Supercritical Water Gasification of Nano-Nickel (Ni^{2+}) Impregnated Biomass for H_2 Production. *Ind. Eng. Chem. Res.* **2019**, *58*, 4780–4793. [CrossRef]
19. Kumar, A.; Reddy, S.N. Subcritical and supercritical water in-situ gasification of metal (Ni/Ru/Fe) impregnated banana pseudo-stem for hydrogen rich fuel gas mixture. *Int. J. Hydrog. Energy* **2019**, *45*, 18348–18362. [CrossRef]
20. Nanda, S.; Reddy, S.N.; Dalai, A.K.; Kozinski, J.A. Subcritical and supercritical water gasification of lignocellulosic biomass impregnated with nickel nanocatalyst for hydrogen production. *Int. J. Hydrog. Energy* **2016**, *41*, 4907–4921. [CrossRef]
21. Bakari, R.; Kivevele, T.; Huang, X.; Jande, Y.A.C. Sub- and Supercritical Water Gasification of Rice Husk: Parametric Optimization Using the I-Optimality Criterion. *ACS Omega* **2021**, *6*, 12480–12499. [CrossRef]
22. Chen, J.; Fan, Y.; Zhao, X.; Jiaqiang, E.; Xu, W.; Zhang, F.; Liao, G.; Leng, E.; Liu, S. Experimental investigation on gasification characteristic of food waste using supercritical water for combustible gas production: Exploring the way to complete gasification. *Fuel* **2020**, *263*, 116735. [CrossRef]
23. Bezerra, M.A.; Santelli, R.E.; Oliveira, E.P.; Villar, L.S.; Escaleira, L.A. Response surface methodology (RSM) as a tool for optimization in analytical chemistry. *Talanta* **2008**, *76*, 965–977. [CrossRef]
24. Okolie, J.A. Supercritical Water Gasification of Lignocellulosic Biomass Materials for Hydrogen Production. Ph.D. Thesis, University of Saskatchewan, Saskatoon, SK, Canada, 2021.
25. Khanal, M.; Rai, D.; Khanal, R.; Bhattarai, A. Determination of point zero charge (PZC) of homemade charcoals of shorea robusta (Sakhuwa) and pinus roxburghii (Salla). *Int. J. Eng. Res. Technol. (IJERT)* **2020**, *9*, 2278-0181.
26. Borges, A.; Onwudili, J.; Andrade, H.; Alves, C.; Ingram, A.; de Melo, S.V.; Torres, E. Catalytic supercritical water gasification of eucalyptus wood chips in a batch reactor. *Fuel* **2019**, *255*, 115804. [CrossRef]
27. Cao, W.; Guo, L.; Yan, X.; Zhang, D.; Yao, X. Assessment of sugarcane bagasse gasification in supercritical water for hydrogen production. *Int. J. Hydrog. Energy* **2018**, *43*, 13711–13719. [CrossRef]
28. Louw, J. Supercritical Water Gasification of Wood-Related Products: A Thermodynamic and Experimental Study. Ph.D. Thesis, Stellenbosch University, Stellenbosch, South Africa, 2016.
29. Kleinübing, S.J.; Vieira, R.S.; Beppu, M.M.; Guibal, E.; Da Silva, M.G.C. Characterization and evaluation of copper and nickel biosorption on acidic algae Sargassum Filipendula. *Mater. Res.* **2010**, *13*, 541–550. [CrossRef]
30. Kuncoro, E.P.; Isnadina, D.R.M.; Darmokoesoemo, H.; Fauziah, O.R.; Kusuma, H.S. Characterization, kinetic, and isotherm data for adsorption of Pb^{2+} from aqueous solution by adsorbent from mixture of bagasse-bentonite. *Data Brief* **2018**, *16*, 622–629. [CrossRef]
31. da Silva, J.C.G.; Alves, J.L.F.; de Araujo Galdino, W.V.; de Sena, R.F.; Andersen, S.L.F. Pyrolysis kinetics and physicochemical characteristics of skin, husk, and shell from green coconut wastes. *Energy Ecol. Environ.* **2019**, *4*, 125–132. [CrossRef]
32. García, R.; Pizarro, C.; Lavín, A.G.; Bueno, J.L. Characterization of Spanish biomass wastes for energy use. *Bioresour. Technol.* **2012**, *103*, 249–258. [CrossRef]
33. Sturion, J.A.; Pereira, J.C.D.; Chemin, M. Qualidade da madeira de Eucalyptus viminalis para fins energéticos em função do espaçamento e idade de corte. *Bol. De Pesqui. Florestal.* **1998**, *16*, 55–59.
34. Said, M.; Cassayre, L.; Dirion, J.-L.; Joulia, X.; Nzihou, A. Effect of Nickel Impregnation on Wood Gasification Mechanism. *Waste Biomass-Valoriz.* **2017**, *8*, 2843–2852. [CrossRef]
35. Singha, R.K.; Yadav, A.; Agrawal, A.; Shukla, A.; Adak, S.; Sasaki, T.; Bal, R. Synthesis of highly coke resistant Ni nanoparticles supported MgO/ZnO catalyst for reforming of methane with carbon dioxide. *Appl. Catal. B Environ.* **2016**, *191*, 165–178. [CrossRef]
36. Devi, T.G.; Kannan, M.P. X-ray Diffraction (XRD) Studies on the Chemical States of Some Metal Species in Cellulosic Chars and the Ellingham Diagrams. *Energy Fuels* **2007**, *21*, 596–601. [CrossRef]
37. Koltypin, Y.; Fernandez, A.; Rojas, T.C.; Campora, J.; Palma, P.; Prozorov, R.; Gedanken, A. Encapsulation of nickel nanoparticles in carbon obtained by the sonochemical decomposition of $Ni(C_8H_{12})_2$. *Chem. Mater.* **1999**, *11*, 1331–1335. [CrossRef]
38. Rout, T.; Pradhan, D.; Singh, R.; Kumari, N. Exhaustive study of products obtained from coconut shell pyrolysis. *J. Environ. Chem. Eng.* **2016**, *4*, 3696–3705. [CrossRef]
39. Sarki, J.; Hassan, S.; Aigbodion, V.; Oghenevweta, J. Potential of using coconut shell particle fillers in eco-composite materials. *J. Alloys Compd.* **2011**, *509*, 2381–2385. [CrossRef]
40. Salavati-Niasari, M.; Mir, N.; Davar, F. A novel precursor in preparation and characterization of nickel oxide nanoparticles via thermal decomposition approach. *J. Alloys Compd.* **2010**, *493*, 163–168. [CrossRef]

41. Ingham, B.; Toney, M.F. X-ray diffraction for characterizing metallic films. In *Metallic Films for Electronic, Optical and Magnetic Applications: Structure, Processing and Properties*; Elsevier: Amsterdam, The Netherlands, 2014; pp. 3–38.
42. Saleh, T.A. *Polymer Hybrid Materials and Nanocomposites: Fundamentals and Applications*; William Andrew: New York, NY, USA, 2021.
43. Saleh, T.A.; Gupta, V.K. *Nanomaterial and Polymer Membranes: Synthesis, Characterization, and Applications*; Elsevier: Amsterdam, The Netherlands, 2016.
44. Chan, F.L.; Tanksale, A. Review of recent developments in Ni-based catalysts for biomass gasification. *Renew. Sustain. Energy Rev.* **2014**, *38*, 428–438. [CrossRef]
45. Lazim, Z.M.; Hadibarata, T.; Puteh, M.H.; Yusop, Z. Adsorption Characteristics of Bisphenol A onto Low-Cost Modified Phyto-Waste Material in Aqueous Solution. *Water Air Soil Pollut.* **2015**, *226*, 34. [CrossRef]
46. Liyanage, C.D.; Pieris, M. A Physico-Chemical Analysis of Coconut Shell Powder. *Procedia Chem.* **2015**, *16*, 222–228. [CrossRef]
47. Orooji, Y.; Ghanbari, M.; Amiri, O.; Salavati-Niasari, M. Facile fabrication of silver iodide/graphitic carbon nitride nanocomposites by notable photo-catalytic performance through sunlight and antimicrobial activity. *J. Hazard. Mater.* **2020**, *389*, 122079. [CrossRef] [PubMed]
48. Okolie, J.; Rana, R.; Nanda, S.; Dalai, A.K.; Kozinski, J.A. Supercritical water gasification of biomass: A state-of-the-art review of process parameters, reaction mechanisms and catalysis. *Sustain. Energy Fuels* **2019**, *3*, 578–598. [CrossRef]
49. Amrullah, A.; Matsumura, Y. Supercritical water gasification of sewage sludge in continuous reactor. *Bioresour. Technol.* **2018**, *249*, 276–283. [CrossRef]
50. Samiee-Zafarghandi, R.; Karimi-Sabet, J.; Abdoli, M.A.; Karbassi, A. Supercritical water gasification of microalga Chlorella PTCC 6010 for hydrogen production: Box-Behnken optimization and evaluating catalytic effect of MnO_2/SiO_2 and NiO/SiO_2. *Renew. Energy* **2018**, *126*, 189–201. [CrossRef]
51. Elif, D.; Nezihe, A. Hydrogen production by supercritical water gasification of fruit pulp in the presence of Ru/C. *Int. J. Hydrog. Energy* **2016**, *41*, 8073–8083. [CrossRef]
52. Demirel, E.; Erkey, C.; Ayas, N. Supercritical Water Gasification of Fruit Pulp for Hydrogen Production: Effect of Reaction Parameters. *J. Supercrit. Fluids* **2021**, *177*, 105329. [CrossRef]
53. Wang, C.; Li, L.; Chen, Y.; Ge, Z.; Jin, H. Supercritical water gasification of wheat straw: Composition of reaction products and kinetic study. *Energy* **2021**, *227*, 120449. [CrossRef]
54. Baig, M.; Leeke, G.; Hammond, P.; Santos, R. Modelling the extraction of soil contaminants with supercritical carbon dioxide. *Environ. Pollut.* **2011**, *159*, 1802–1809. [CrossRef]
55. Nanda, S.; Gong, M.; Hunter, H.N.; Dalai, A.K.; Gökalp, I.; Kozinski, J.A. An assessment of pinecone gasification in subcritical, near-critical and supercritical water. *Fuel Process. Technol.* **2017**, *168*, 84–96. [CrossRef]
56. Su, H.; Kanchanatip, E.; Wang, D.; Zhang, H.; Antoni; Mubeen, I.; Huang, Z.; Yan, M. Catalytic gasification of food waste in supercritical water over La promoted Ni/Al_2O_3 catalysts for enhancing H_2 production. *Int. J. Hydrog. Energy* **2020**, *45*, 553–564. [CrossRef]
57. Williams, P.T.; Onwudili, J. Composition of Products from the Supercritical Water Gasification of Glucose: A Model Biomass Compound. *Ind. Eng. Chem. Res.* **2005**, *44*, 8739–8749. [CrossRef]
58. Borges, A.C.P. Gaseificação de Cavaco de Eucalipto em Água Supercrítica na Presença do Catalisador $NiFe_2O_4$. 2021. Available online: https://repositorio.ufba.br/handle/ri/32553 (accessed on 1 April 2023).
59. Nanda, S.; Reddy, S.N.; Hunter, H.N.; Vo, D.-V.N.; Kozinski, J.A.; Gökalp, I. Catalytic subcritical and supercritical water gasification as a resource recovery approach from waste tires for hydrogen-rich syngas production. *J. Supercrit. Fluids* **2019**, *154*, 104627. [CrossRef]
60. Adar, E.; Ince, M.; Bilgili, M.S. Supercritical water gasification of sewage sludge by continuous flow tubular reactor: A pilot scale study. *Chem. Eng. J.* **2020**, *391*, 123499. [CrossRef]
61. Wang, C.; Jin, H.; Feng, H.; Wei, W.; Cao, C.; Cao, W. Study on gasification mechanism of biomass waste in supercritical water based on product distribution. *Int. J. Hydrog. Energy* **2020**, *45*, 28051–28061. [CrossRef]
62. Ruya, P.M.; Purwadi, R.; Lim, S.S. Supercritical water gasification of sewage sludge for power generation–thermodynamic study on auto-thermal operation using Aspen Plus. *Energy Convers. Manag.* **2020**, *206*, 112458. [CrossRef]
63. Yildirir, E.; Ballice, L. Supercritical water gasification of wet sludge from biological treatment of textile and leather industrial wastewater. *J. Supercrit. Fluids* **2019**, *146*, 100–106. [CrossRef]
64. Nanda, S.; Reddy, S.N.; Vo, D.-V.N.; Sahoo, B.N.; Kozinski, J.A. Catalytic gasification of wheat straw in hot compressed (subcritical and supercritical) water for hydrogen production. *Energy Sci. Eng.* **2018**, *6*, 448–459. [CrossRef]
65. Basu, P. *Biomass Gasification and Pyrolysis: Practical Design and Theory*; Academic Press: Cambridge, MA, USA, 2010.
66. Alam, M.A.; Hamdan, H.Y.; Azeem, M.; Hussain, P.B.; bin Salit, M.S.; Khan, R.; Arif, S.; Ansari, A.H. Modelling and optimisation of hardness behaviour of sintered Al/SiC composites using RSM and ANN: A comparative study. *J. Mater. Res. Technol.* **2020**, *9*, 14036–14050. [CrossRef]
67. Abdpour, S.; Santos, R.M. Recent advances in heterogeneous catalysis for supercritical water oxidation/gasification processes: Insight into catalyst development. *Process. Saf. Environ. Prot.* **2021**, *149*, 169–184. [CrossRef]
68. Zhang, J.; Dasgupta, A.; Chen, Z.; Xu, D.; Savage, P.E.; Guo, Y. Supercritical water gasification of phenol over Ni-Ru bimetallic catalysts. *Water Res.* **2019**, *152*, 12–20. [CrossRef]

69. Resende, F.L.P.; Savage, P.E. Effect of Metals on Supercritical Water Gasification of Cellulose and Lignin. *Ind. Eng. Chem. Res.* **2010**, *49*, 2694–2700. [CrossRef]
70. Pairojpiriyakul, T.; Croiset, E.; Kiatkittipong, K.; Kiatkittipong, W.; Arpornwichanop, A.; Assabumrungrat, S. Catalytic reforming of glycerol in supercritical water with nickel-based catalysts. *Int. J. Hydrog. Energy* **2014**, *39*, 14739–14750. [CrossRef]